Available online at www.sciencedirect.com
SCIENCE DIRECT®
ELSEVIER
International Journal of Solids and Structures 43 (2006) 1459–1489
INTERNATIONAL JOURNAL OF SOLIDS and STRUCTURES
www.elsevier.com/locate/ijsolstr

Bonded lap joints of composite laminates with tapered edges

E. Oterkus [a], A. Barut [a], E. Madenci [a,*], S.S. Smeltzer III [b], D.R. Ambur [c]

[a] *Department of Aerospace and Mechanical Engineering, The University of Arizona, 1130 N. Mountain Avenue, Tucson, AZ 85721, USA*
[b] *NASA Langley Research Center, Hampton, VA 23681, USA*
[c] *NASA Glenn Research Center, Cleveland, OH 44135, USA*

Received 18 November 2004; received in revised form 1 July 2005
Available online 12 September 2005

Abstract

This study presents a semi-analytical solution method to analyze the geometrically nonlinear response of bonded composite lap joints with tapered and/or non tapered adherend edges under uniaxial tension. The solution method provides the transverse shear and normal stresses in the adhesives and in-plane stress resultants and bending moments in the adherends. The method utilizes the principle of virtual work in conjunction with von Karman's nonlinear plate theory to model the adherends and the shear lag model to represent the kinematics of the thin adhesive layers between the adherends. Furthermore, the method accounts for the bilinear elastic material behavior of the adhesive while maintaining a linear stress–strain relationship in the adherends. In order to account for the stiffness changes due to thickness variation of the adherends along the tapered edges, the in-plane and bending stiffness matrices of the adherents are varied as a function of thickness along the tapered region. The combination of these complexities results in a system of nonlinear governing equilibrium equations. This approach represents a computationally efficient alternative to finite element method. The numerical results present the effects of taper angle, adherend overlap length, and the bilinear adhesive material on the stress fields in the adherends, as well as the adhesives of a single- and double-lap joint.

Keywords: Bonded; Lap joints; Nonlinear; Laminates

1. Introduction

The reduction of the transverse shear and normal stress concentrations along the edges of adhesive bond lines is important in order to prevent premature failure of the bonded joint. The determination of the complete stress and strain fields in bonded composite lap joints presents difficulties arising from the step-wise

* Corresponding author. Tel.: +1 520 621 6113; fax: +1 520 621 8191.
E-mail address: madenci@email.arizona.edu (E. Madenci).

0020-7683/$ - see front matter © 2005 Elsevier Ltd. All rights reserved.
doi:10.1016/j.ijsolstr.2005.07.035

geometry, material property variations, laminated construction of the adherends, the bilinear material behavior of the adhesive, as well as the effect of tension induced stiffening (geometrically nonlinear effect) on the bending deformation of the adherends subjected to uniaxial tension. Also, the local stress variations near the ends of the overlap region are characterized by very high gradients or even analytically predicted singularities. The sharp gradients of the stress components depend on the elastic properties of the adherends and adhesive as well as the joint geometry. These peak transverse normal and shear stresses in the adhesive can be reduced by tapering the adherends toward the ends.

In order to facilitate the use of lap joints in present and future structures, the analysis of the geometrically nonlinear response of bonded single-lap joints has received considerable attention over the past two decades. Previous analyses of bonded lap joints can be categorized as "shear-lag" and "finite-element" models. An extensive review and in-depth discussion of the previous investigations can be found in articles by Tsai and Morton (1994), Ding and Kumosa (1994) and Osnes and Andersen (2003). Due to the aforementioned complexities, the majority of the investigations have utilized the finite element method in determining the stress and the strain field in a bonded lap joint. However, in many of these investigations, the three-dimensional description of the bonded lap joint was simplified to a two-dimensional analysis under certain assumptions (Dattaguru et al., 1984; Reddy and Roy, 1988; Pandey et al., 1999; Apalak and Gunes, 2001).

In order to enhance computational efficiency, Penado (1998) introduced an approach based on the substructuring technique. In this approach, the general response of the bonded lap joint is obtained analytically from the solution of force-moment equilibrium conditions. The analytically evaluated force-moment values at the overlap ends are then used as the natural boundary condition for a highly detailed two-dimensional finite element analysis of the overlap joint under the assumption that the overlap ends are simply supported.

Combining the shear-lag model of Goland and Reissner (1944) with a detailed finite element modeling of the adherends with three-dimensional elements, Edlund and Klarbring (1992) employed the principle of virtual work to analyze the geometrically nonlinear response of bonded single-lap joints with a linearly elastic adhesive. The shear-lag model approximates the transverse shear and normal strain components in terms of the relative displacements of the adherends. An alternative to the shear-lag model is to model the adhesive with one or two layers of brick elements and assemble these elements with the brick elements of the adherends. However, as mentioned before, the size of the brick elements used in the adhesive might introduce aspect ratio problems. The recent investigations by Pandey and Narasimhan (2001) and Narasimhan and Pandey (2003) utilized this approach for solving the three-dimensional large deflection analysis of single-lap joints with viscoelastic adhesive behavior.

In the finite element analysis, the adhesive requires a highly refined mesh in order to keep the proper aspect ratio between the elements in the adherends and adhesive. Therefore, the major advantage of the two-dimensional finite element models over the three-dimensional models is the significant reduction of the number of degrees of freedom. Furthermore, for an incremental-iterative solution of the governing equations in which the global stiffness matrix is repeatedly calculated, the three-dimensional finite element analysis of the entire domain becomes computationally demanding.

Thus, it is beneficial to have an efficient special-purpose analysis method that can be used to conduct extensive parametric studies in a timely manner and at relatively low computational costs. However, there is no analytical or semi-analytical approach for determining the three-dimensional response of the geometrically nonlinear analysis of bonded single-lap joints. Therefore, the goal of the present study is to develop a three-dimensional analysis method that is well suited for parametric studies that accurately predicts the geometrically nonlinear behavior of a composite lap joint with tapered edges subjected to uniaxial tension. In particular, this study focuses on the effects of geometric nonlinearity, tapering of the adherend thickness, changes in the overlap length of the adherends, and the linear and bilinear elastic behaviors of the adhesive on the in-plane stresses in the adherends and the transverse normal and transverse shear stresses in the adhesive of the joint.

In the remainder of this paper, details of the analysis method are presented and results from this approach are discussed. First, the boundary-value problem is defined. Next, the analysis details and numerical solution procedure are described. Then, results for two bonded lap-joint configurations are presented.

2. Problem statement

The bonded lap joint configurations consists of two or more rectangular composite adherends and thin adhesive layers in between them, as shown in Fig. 1. While the adhesive thickness is uniform, the composite adherends may have tapered edges. The tapered edges of the adherends are used to reduce stress concentrations along the edges. A lap joint may consist of P number of adherends which are bonded to each other by adhesive layers. The adherends are identified by sub- or super-script, (p) with $p = 1, \ldots, P$. As shown in Fig. 1, each adhesive layer (interface) between the two adjacent adherends denoted by (i) and (j) is identified by superscript, (i, j). The area and boundary of the pth adherend are denoted by $A^{(p)}$ and $\Gamma^{(p)}$, respectively. The area and boundary of the adhesive (interface) between the ith and jth adherends are denoted by $A^{(i,j)}$ and $\Gamma^{(i,j)}$, respectively. As shown in Fig. 1, both the adherends and adhesive layers (interfaces) have rectangular boundary geometries. Hence, their boundaries can be represented by four straight boundary segments, i.e,

$$\Gamma^{(p)} = \sum_{m=1}^{4} \Gamma_m^{(p)} \quad \text{and} \quad \Gamma^{(i,j)} = \sum_{m=1}^{4} \Gamma_m^{(i,j)} \tag{1}$$

in which $\Gamma_m^{(p)}$ and $\Gamma_m^{(i,j)}$ denote the mth boundary segment around the adherend and interface (adhesive). Along the adherend and adhesive boundaries, the unit normals to the mth boundary segment are represented by $\mathbf{n}_m^{(p)}$ and $\mathbf{n}_m^{(i,j)}$ as depicted in Fig. 1.

Although the current analysis addresses bonded lap joints under uniaxial tension only, the formulation includes general loading conditions. Therefore, the exterior edges of the adherends can be subjected to both in-plane tractions and bending moments. The in-plane external tractions include components, t_x, t_y, and t_z, and the external bending tractions include components m_x and m_y. In the adherends, the global displacement components in the x-, y-, and z-directions are denoted by, $U_x^{(p)}$, $U_y^{(p)}$, and $U_z^{(p)}$, respectively $(p = 1, \ldots, P)$.

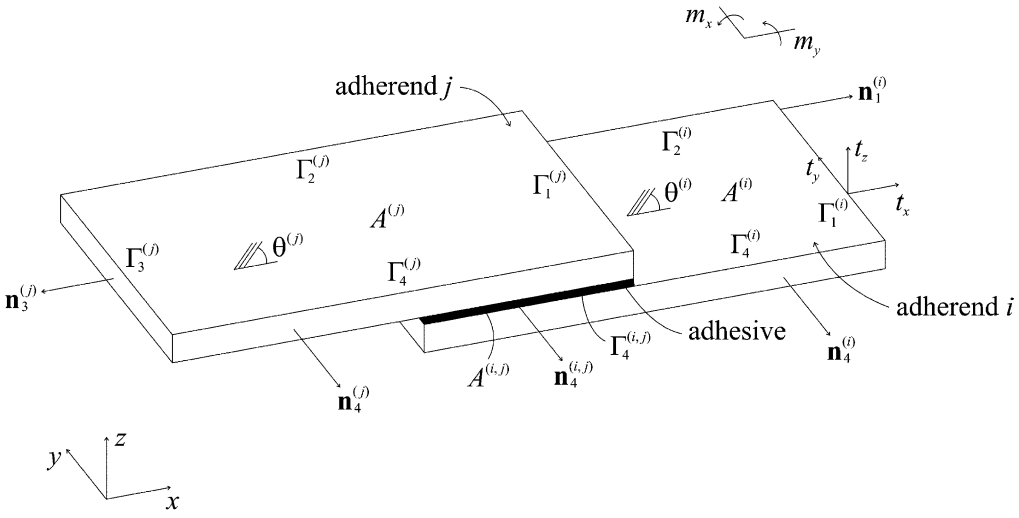

Fig. 1. Description of geometry, fiber angle, and loading of two adjacent adherends in a bonded lap joint.

The laminated adherends are made of specially orthotropic layers. Each layer has a thickness of $t_k^{(p)}$ and orientation angle of $\theta_k^{(p)}$, $(p = 1, \ldots, P)$, which is defined with respect to the positive x-axis. Also, the orthotropic material properties of each layer include the elastic moduli, $E_L^{(p)}$ and $E_T^{(p)}$, shear modulus $G_{LT}^{(p)}$, and Poisson's ratio $v_{LT}^{(p)}$, where L and T are the longitudinal (fiber) and transverse directions, respectively. The adhesive material between the ith and jth adherends is isotropic, homogeneous, and elastic with a bilinear relation for the effective transverse shear stress, $\tau_{\text{eff}}^{(i,j)}$, and effective transverse shear strain, $\gamma_{\text{eff}}^{(i,j)}$, as shown in Fig. 2. The effective transverse shear stress and strain in the adhesive between the ith and jth adherends are defined by

$$\tau_{\text{eff}}^{(i,j)} = \sqrt{\sigma_{xz}^{(i,j)^2} + \sigma_{yz}^{(i,j)^2}} \tag{2b}$$

$$\gamma_{\text{eff}}^{(i,j)} = \sqrt{\gamma_{xz}^{(i,j)^2} + \gamma_{yz}^{(i,j)^2}} \tag{2c}$$

in which $\sigma_{xz}^{(i,j)}$ and $\sigma_{yz}^{(i,j)}$ represent the components of the transverse shear stress and $\gamma_{xz}^{(i,j)}$ and $\gamma_{yz}^{(i,j)}$ represent the components of the transverse shear strain in the adhesive. As shown in Fig. 2, the initial shear modulus of the bilinear adhesive behavior is denoted by $G_1^{(i,j)}$, and it reduces to $G_2^{(i,j)}$ when the effective transverse shear strain, $\gamma_{\text{eff}}^{(i,j)}$, reaches the characteristic shear strain, $\gamma_c^{(i,j)}$. Also, it has a Poisson's ratio of $v^{(i,j)}$. With these parameters, the bilinear relationship between the effective transverse shear stress, $\tau_{\text{eff}}^{(i,j)}$, and effective transverse shear strain, $\gamma_{\text{eff}}^{(i,j)}$, can be expressed as

$$\tau_{\text{eff}}^{(i,j)} = G_1^{(i,j)}\gamma_{\text{eff}}^{(i,j)}[1 - H(\gamma_{\text{eff}}^{(i,j)} - \gamma_c^{(i,j)})] + [G_1^{(i,j)}\gamma_c^{(i,j)} + G_2^{(i,j)}(\gamma_{\text{eff}}^{(i,j)} - \gamma_c^{(i,j)})] \times H(\gamma_{\text{eff}}^{(i,j)} - \gamma_c^{(i,j)}) \tag{3}$$

where $H(\gamma_{\text{eff}}^{(i,j)} - \gamma_c^{(i,j)})$ is the Heaviside step function.

In accordance with this relationship, the transverse shear stresses, $\sigma_{\alpha z}^{(i,j)}$, and strains, $\gamma_{\alpha z}^{(i,j)}$, are related by

$$\sigma_{\alpha z}^{(i,j)} = G_{\text{eff}}^{(i,j)}\gamma_{\alpha z}^{(i,j)}(\alpha = x, y) \tag{4}$$

in which the parameters $G_{\text{eff}}^{(i,j)}$ represent the effective shear modulus of the adhesive layer, defined as

$$G_{\text{eff}}^{(i,j)} = \frac{\tau_{\text{eff}}^{(i,j)}}{\gamma_{\text{eff}}^{(i,j)}} \tag{5}$$

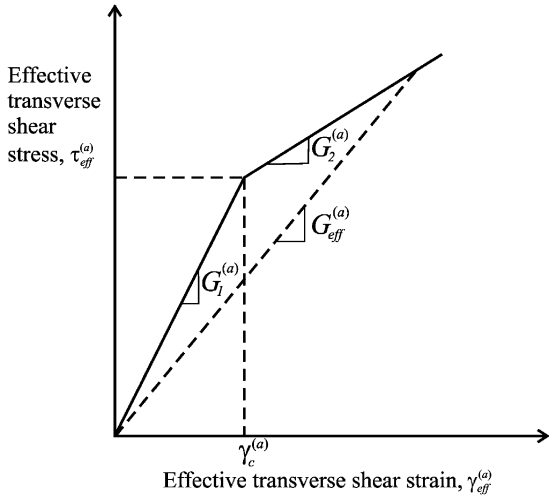

Fig. 2. Bilinear behavior of the adhesive in terms of effective transverse shear stress and transverse shear strain.

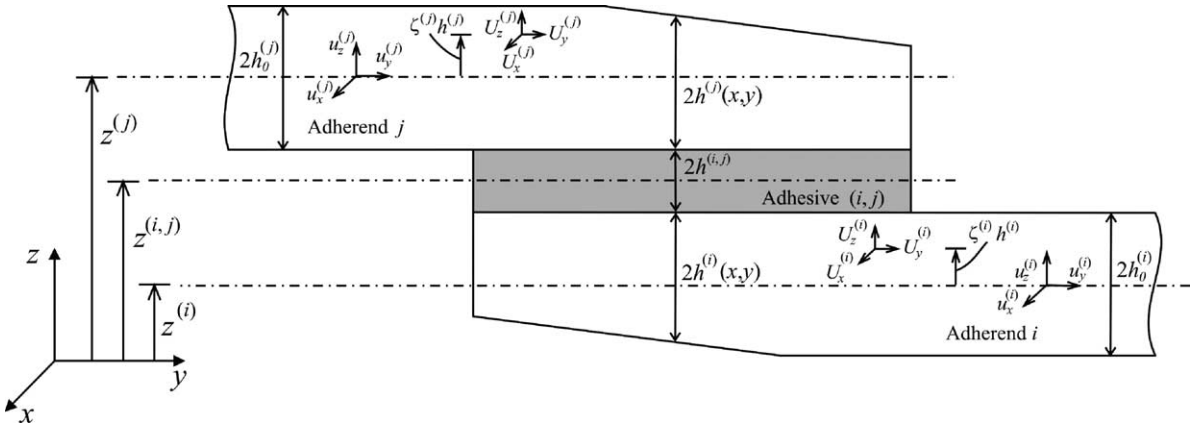

Fig. 3. The reference surface and kinematics of a bonded lap joint.

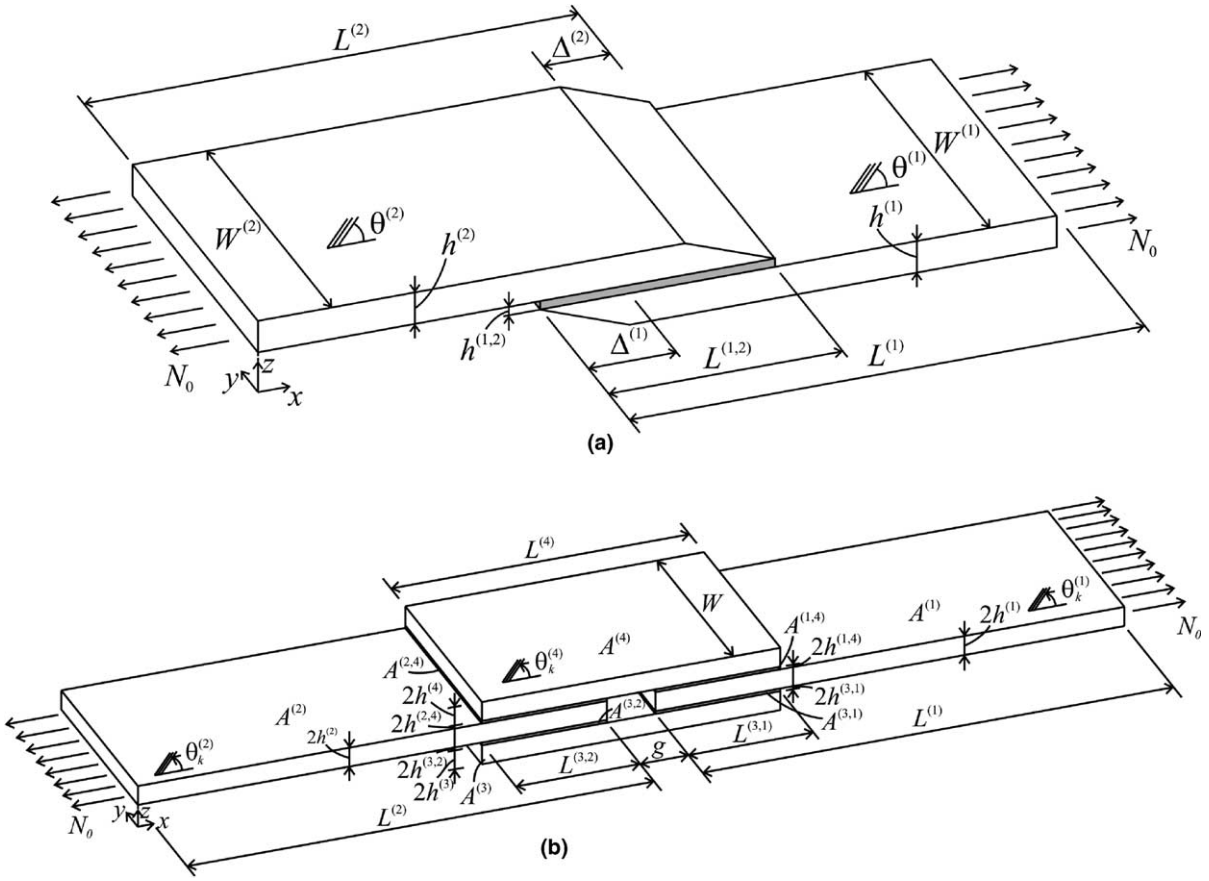

Fig. 4. Description of lap joint geometry and loading: (a) single-lap and (b) double-lap.

Furthermore, the transverse normal stress, $\sigma_{zz}^{(i,j)}$, and strain, $\varepsilon_{zz}^{(i,j)}$, in the adhesive are related by

$$\sigma_{zz}^{(i,j)} = E_{\text{eff}}^{(i,j)} \varepsilon_{zz}^{(i,j)} \tag{6}$$

in which $E_{\text{eff}}^{(i,j)}$ is the effective Young's modulus expressed as

$$E_{\text{eff}}^{(i,j)} = 2G_{\text{eff}}^{(i,j)}(1 + v^{(i,j)}) \tag{7}$$

While the thickness of the adhesive between the ith and jth adherends is uniform and denoted by $2h^{(i,j)}$, the adherends have variable thicknesses, $2h^{(p)}(x, y)$, with $(p = 1, \ldots, P)$, due to their tapered shape near the edges. The thicknesses of the adherends are defined as discrete linear functions of the in-plane coordinates. The reference planes of the pth adherend and the adhesive (interface) between the ith and jth adherends are, respectively, denoted by $z^{(p)}$ and $z^{(i,j)}$ as shown in Fig. 3.

The problem posed here concerns the development of a three-dimensional semi-analytical method to determine the displacement and stress fields in bonded lap joints while including the effects of geometric nonlinearity and bilinear elastic adhesive material behavior. The capability of the method is demonstrated by considering first a single-lap joint of quasi-isotropic tapered adherends and a bilinear adhesive material behavior as illustrated in Fig. 4a. The second configuration concerns a double-lap joint consisting four adherends bonded with linear or bilinear adhesives as illustrated in Fig. 4b. The lap joints are simply supported along the left and right edges of the upper and lower adherends, respectively. The left edge of the upper adherend is also restrained against any horizontal movement. Furthermore, the mid points of the left and right edges of the lower and upper adherends are restrained to move in the y-direction so as to suppress the rigid-body movement of the lap joint.

3. Solution method

The present three-dimensional geometrically nonlinear analysis method is based on the principle of virtual work. The displacement components are approximated in terms of the B-spline functions (Hoschek and Lasser, 1993) in a double series representation as

$$u_{\alpha}^{(p)} = \sum_{m=0}^{M_x^{(p)}} \sum_{n=0}^{M_y^{(p)}} c_{\alpha(mn)}^{(p)} T_m(x; \mathbf{t}_x^{(p)}, K) T_n(y; \mathbf{t}_y^{(p)}, K) \tag{8}$$

in which $c_{\alpha(mn)}^{(p)}$, with $(p = 1, \ldots, P)$ and $(\alpha = x, y, z)$, are the unknown coefficients. The parameter $M_{\beta}^{(p)}$, with $(\beta = x, y)$ specifies the extent of the series and the knot vector $\mathbf{t}_{\beta}^{(p)}$ contains pre-selected knot points (coordinates) in the direction of β. These knot points are used to increase the accuracy of the B-splines at certain locations. Also, the parameter K controls the degree of the B-spline functions and, consequently, the continuity of the field variable. The Kth-order B-spline function is comprised of the $(K-1)$th-order of polynomials. The details of the B-spline functions along with the definitions of the parameters $\mathbf{t}_{\beta}^{(p)}$ and K are given in Appendix A. These displacement functions can be expressed in matrix form as

$$u_x^{(p)} = \mathbf{V}^{(p)^{\mathrm{T}}} \mathbf{c}_x^{(p)} \tag{9a}$$

$$u_y^{(p)} = \mathbf{V}^{(p)^{\mathrm{T}}} \mathbf{c}_y^{(p)} \tag{9b}$$

$$u_z^{(p)} = \mathbf{V}^{(p)^{\mathrm{T}}} \mathbf{c}_z^{(p)} \tag{9c}$$

in which the vectors $\mathbf{c}_{\alpha}^{(p)}$, with $(\alpha = x, y, z)$, contain the unknown coefficients (generalized coordinates) $c_{\alpha(mn)}^{(p)}$. The known vectors, $\mathbf{V}^{(p)}$, are expressed in terms of the B-spline functions $T_m(x; \mathbf{t}_x^{(p)}, K)$ and $T_n(y; \mathbf{t}_y^{(p)}, K)$. In matrix form, the approximate displacement representations of Eqs. (9a)–(9c) are rewritten as

$$u_x^{(p)} = \mathbf{V}_x^{(p)^{\mathrm{T}}}\mathbf{q}^{(p)}$$
$$u_y^{(p)} = \mathbf{V}_y^{(p)^{\mathrm{T}}}\mathbf{q}^{(p)} \tag{10}$$
$$u_z^{(p)} = \mathbf{V}_z^{(p)^{\mathrm{T}}}\mathbf{q}^{(p)}$$

in which the known vectors, $\mathbf{V}_\alpha^{(p)}$, with $(\alpha = x, y, z)$, are defined as

$$\mathbf{V}_x^{(p)^{\mathrm{T}}} = \left\{\mathbf{V}^{(p)}, \mathbf{0}, \mathbf{0}\right\} \tag{11a}$$
$$\mathbf{V}_y^{(p)^{\mathrm{T}}} = \left\{\mathbf{0}, \mathbf{V}^{(p)}, \mathbf{0}\right\} \tag{11b}$$
$$\mathbf{V}_z^{(p)^{\mathrm{T}}} = \left\{\mathbf{0}, \mathbf{0}, \mathbf{V}^{(p)}\right\} \tag{11c}$$

The unknown vector $\mathbf{q}^{(p)}$ is defined as

$$\mathbf{q}^{(p)^{\mathrm{T}}} = \left\{\mathbf{c}_x^{(p)^{\mathrm{T}}}, \mathbf{c}_y^{(p)^{\mathrm{T}}}, \mathbf{c}_z^{(p)^{\mathrm{T}}}\right\} \tag{12}$$

Note that the series representation of the displacement components is not required to satisfy any type of kinematic admissibility.

3.1. Displacement components

The adherends interacting through the adhesive, which sustains transverse normal and shear deformations but not in-plane deformation, experience in-plane and bending deformations while the transverse normal and shear deformations are disregarded because the adherends are considered to be thin. Therefore, the in-plane strain components in the adhesive, and the transverse normal and shear strain components in the adherends, are not included in the derivation of the kinematic relations.

In accordance with the Kirchhoff plate theory, the global displacement components, $U_x^{(p)}$, $U_y^{(p)}$, and $U_z^{(p)}$ in each of the adherends are defined as

$$U_\alpha^{(p)}(x, y, z) = u_\alpha^{(p)}(x, y) - \zeta^{(p)} h^{(p)} u_{z,\alpha}^{(p)} \tag{13a}$$
$$U_z^{(p)}(x, y, z) = u_z^{(p)}(x, y) \tag{13b}$$

for which $(p = 1, \ldots, P)$ and $(\alpha = x, y)$, and the displacement components, $u_x^{(p)}$, $u_y^{(p)}$, and $u_z^{(p)}$, are defined on the reference surfaces with respect to the global Cartesian coordinates $(x^{(p)}, y^{(p)}, z^{(p)})$. In Eq. (13), the subscript after a comma indicates differentiation with respect to the variable. The coordinate $\zeta^{(p)}$ located on each of the reference planes is defined as

$$\zeta^{(p)} = \frac{z - z^{(p)}}{h^{(p)}} \quad (p = 1, \ldots, P) \tag{14}$$

and varies in the range $-1 \leqslant \zeta^{(p)} \leqslant 1$, with $(p = 1, \ldots, P)$. The thicknesses of the adherends are specified by $2h^{(p)}(x, y)$, in which $2h^{(p)}(x, y) = 2h_0^{(p)}$ in the untapered sections of the adherends. Also, the location of the reference planes with respect to the global coordinate system (x, y, z) are defined by $z^{(p)}$, which are located at the mid-surfaces (with respect to the untapered thickness) of the adherends.

3.2. Strain–displacement relations

The strain measure for the adherends is based on the modified form of Green's nonlinear strain displacement relations in conjunction with von Karman assumptions for large deformation of plates (Fung and

Tong, 2001). Therefore, the strain components in the adherends, $e_{\alpha\beta}^{(p)}$ $(p = 1, \ldots, P; \alpha, \beta = x, y)$, can be expressed as

$$e_{xx}^{(p)} = \varepsilon_{xx}^{(p)} + \zeta^{(p)} h^{(p)} \kappa_{xx}^{(p)} + \frac{1}{2}(u_{z,x}^{(p)})^2 \tag{15a}$$

$$e_{yy}^{(p)} = \varepsilon_{yy}^{(p)} + \zeta^{(p)} h^{(p)} \kappa_{yy}^{(p)} + \frac{1}{2}(u_{z,y}^{(p)})^2 \tag{15b}$$

$$e_{xy}^{(p)} = \frac{1}{2}\gamma_{xy}^{(p)} + \frac{1}{2}\zeta^{(p)} h^{(p)} \kappa_{xy}^{(p)} + \frac{1}{2} u_{z,x}^{(p)} u_{z,y}^{(p)} \tag{15c}$$

in which

$$\varepsilon_{xx}^{(p)} = u_{x,x}^{(p)}; \kappa_{xx}^{(p)} = -u_{z,xx}^{(p)} \tag{16a, b}$$

$$\varepsilon_{yy}^{(p)} = u_{y,y}^{(p)}; \kappa_{yy}^{(p)} = -u_{z,yy}^{(p)} \tag{16c, d}$$

$$\gamma_{xy}^{(p)} = u_{x,y}^{(p)} + u_{y,x}^{(p)}; \kappa_{xy}^{(p)} = -2u_{z,xy}^{(p)} \tag{16e, f}$$

where $\varepsilon_{xx}^{(p)}$, $\varepsilon_{yy}^{(p)}$, and $\gamma_{xy}^{(p)}$ represent the in-plane strain resultants and $\kappa_{xx}^{(p)}$, $\kappa_{yy}^{(p)}$, and $\kappa_{xy}^{(p)}$ represent the bending strain (curvature) resultants on the reference surfaces. Also, the in-plane and bending (curvature) strain resultants constitute the components of the linear part of the in-plane strain, $\boldsymbol{\varepsilon}_L^{(p)}$, and curvature, $\boldsymbol{\kappa}_L^{(p)}$, vectors in the form

$$\boldsymbol{\varepsilon}_L^{(p)^{\mathrm{T}}} = \left\{ \varepsilon_{xx}^{(p)}, \varepsilon_{yy}^{(p)}, \gamma_{xy}^{(p)} \right\} = \left\{ u_{x,x}^{(p)}, u_{y,y}^{(p)}, u_{x,y}^{(p)} + u_{y,x}^{(p)} \right\} \tag{17a}$$

$$\boldsymbol{\kappa}_L^{(p)^{\mathrm{T}}} = \left\{ \kappa_{xx}^{(p)}, \kappa_{yy}^{(p)}, \kappa_{xy}^{(p)} \right\} = \left\{ -u_{z,xx}^{(p)}, -u_{z,yy}^{(p)}, -2u_{z,xy}^{(p)} \right\} \tag{17b}$$

Similarly, the nonlinear terms appearing in the strain components, $e_{\alpha\beta}^{(p)}$ $(\alpha, \beta = x, y)$, are included in the nonlinear part of the in-plane strain resultant vector, $\boldsymbol{\varepsilon}_N^{(p)}$, in the form

$$\boldsymbol{\varepsilon}_N^{(p)^{\mathrm{T}}} = \left\{ \frac{1}{2}(u_{z,x}^{(p)})^2, \frac{1}{2}(u_{z,y}^{(p)})^2, u_{z,x}^{(p)} u_{z,y}^{(p)} \right\} \tag{18}$$

Although the bending deformations (curvatures) are only linearly related to the out-of-plane displacement component, $u_z^{(p)}$, for consistency, a zero-valued vector is employed to represent the nonlinear part of the curvature vector, $\boldsymbol{\kappa}_N^{(p)}$, as

$$\boldsymbol{\kappa}_N^{(p)} = \{0, 0, 0\} \tag{19}$$

Substituting for the derivatives of the displacement components from Eq. (10), the linear and nonlinear parts of the in-plane strain resultant and curvature vectors can be expressed as

$$\boldsymbol{\varepsilon}_L^{(p)} = \mathbf{L}_{\varepsilon_L}^{(p)} \mathbf{q}^{(p)}, \quad \boldsymbol{\kappa}_L^{(p)} = \mathbf{L}_{\kappa_L}^{(p)} \mathbf{q}^{(p)} \tag{20a, b}$$

$$\boldsymbol{\varepsilon}_N^{(p)} = \mathbf{L}_{\varepsilon_N}^{(p)}(\mathbf{q}^{(p)}) \mathbf{q}^{(p)}, \quad \boldsymbol{\kappa}_N^{(p)} = 0 \tag{20c, d}$$

where

$$\mathbf{L}_{\varepsilon_L}^{(p)} = \begin{bmatrix} \mathbf{V}_{x,x}^{(p)^{\mathrm{T}}} \\ \mathbf{V}_{y,y}^{(p)^{\mathrm{T}}} \\ \mathbf{V}_{x,y}^{(p)^{\mathrm{T}}} + \mathbf{V}_{y,x}^{(p)^{\mathrm{T}}} \end{bmatrix} \tag{21a}$$

$$\mathbf{L}_{\kappa_L}^{(p)} = -\begin{bmatrix} \mathbf{V}_{z,xx}^{(p)^{\mathrm{T}}} \\ \mathbf{V}_{z,yy}^{(p)^{\mathrm{T}}} \\ 2\mathbf{V}_{z,xy}^{(p)^{\mathrm{T}}} \end{bmatrix} \tag{21b}$$

$$\mathbf{L}_{\varepsilon_N}^{(p)}(\mathbf{q}^{(p)}) = \frac{1}{2}\begin{bmatrix} u_{z,x}^{(p)}\mathbf{V}_{z,x}^{(p)^{\mathrm{T}}} \\ u_{z,y}^{(p)}\mathbf{V}_{z,y}^{(p)^{\mathrm{T}}} \\ u_{z,x}^{(p)}\mathbf{V}_{z,y}^{(p)^{\mathrm{T}}} + u_{z,y}^{(p)}\mathbf{V}_{z,x}^{(p)^{\mathrm{T}}} \end{bmatrix} \tag{21c}$$

The vectors of strain resultants defined in Eq. (20) can be combined in a compact form as

$$\mathbf{e}_{\alpha}^{(p)} = \mathbf{L}_{\alpha}^{(p)}\mathbf{q}^{(p)} \quad (\alpha = L, N) \tag{22}$$

where

$$\mathbf{e}_{\alpha}^{(p)^{\mathrm{T}}} = \left\{\boldsymbol{\varepsilon}_{\alpha}^{(p)^{\mathrm{T}}}, \boldsymbol{\kappa}_{\alpha}^{(p)^{\mathrm{T}}}\right\}, \quad \mathbf{L}_{L}^{(p)} = \begin{bmatrix} \mathbf{L}_{\varepsilon_L}^{(p)} \\ \mathbf{L}_{\kappa_L}^{(p)} \end{bmatrix} \tag{23a, b}$$

$$\mathbf{L}_{N}^{(p)}(\mathbf{q}^{(p)}) = \begin{bmatrix} \mathbf{L}_{\varepsilon_N}^{(p)}(\mathbf{q}^{(p)}) \\ 0 \end{bmatrix} \tag{23c}$$

Furthermore, the linear and nonlinear parts of the strain vectors, $\mathbf{e}_{L}^{(p)}$ and $\mathbf{e}_{N}^{(p)}$, can be added to form the total strain vector as

$$\mathbf{e}^{(p)} = \mathbf{e}_{L}^{(p)} + \mathbf{e}_{N}^{(p)} = \left[\mathbf{L}_{L}^{(p)} + \mathbf{L}_{N}^{(p)}(\mathbf{q}^{(p)})\right]\mathbf{q}^{(p)} = \mathbf{H}^{(p)}(\mathbf{q}^{(p)})\mathbf{q}^{(p)} \tag{24}$$

where

$$\mathbf{H}^{(p)}(\mathbf{q}^{(p)}) = \mathbf{L}_{L}^{(p)} + \mathbf{L}_{N}^{(p)}(\mathbf{q}^{(p)}) \tag{25}$$

The displacement components, in the adhesive bonding of the ith and jth adherends, are assumed to vary linearly through the thickness (Tsai and Morton, 1994). Although the adhesive undergoes the same magnitudes of the in-plane and transverse displacements as those of the adherends, the strain measure is based on a linear shear-lag model, where the transverse shear strain and the normal strain components in the interface (adhesive) between the ith and jth adherends are expressed as

$$\gamma_{\alpha z}^{(i,j)} = \frac{1}{2h^{(i,j)}}\left[u_{\alpha}^{(i)}(x,y) - u_{\alpha}^{(j)}(x,y)\right] + \frac{1}{2h^{(i,j)}}\left[h^{(i)}u_{z,\alpha}^{(i)} + h^{(j)}u_{z,\alpha}^{(j)}\right] \quad (\alpha = x, y) \tag{26a}$$

$$\varepsilon_{zz}^{(i,j)} = \frac{1}{2h^{(i,j)}}\left[u_{z}^{(i)}(x,y) - u_{z}^{(j)}(x,y)\right] \tag{26b}$$

Finally, substituting from Eq. (10) for the displacement components in Eq. (26) leads to the strain vector containing the transverse shear and normal strain components in the adhesive as

$$\boldsymbol{\varepsilon}^{(i,j)} = \mathbf{L}_a^{(i)}\mathbf{q}^{(i)} - \mathbf{L}_a^{(j)}\mathbf{q}^{(j)} \tag{27}$$

where

$$\boldsymbol{\varepsilon}^{(i,j)T} = \left\{\gamma_{xz}^{(i,j)}, \gamma_{yz}^{(i,j)}, \varepsilon_{zz}^{(i,j)}\right\} \tag{28}$$

and the matrices $\mathbf{L}_a^{(\alpha)}$ are defined as

$$\mathbf{L}_a^{(i)} = \mathbf{L}_{a\varepsilon}^{(i)} + \mathbf{L}_{a\kappa}^{(i)} \tag{29a}$$

$$\mathbf{L}_a^{(j)} = \mathbf{L}_{a\varepsilon}^{(j)} - \mathbf{L}_{a\kappa}^{(j)} \tag{29b}$$

in which

$$\mathbf{L}_{a\varepsilon}^{(\alpha)} = \frac{1}{2h^{(i,j)}}\begin{bmatrix} \mathbf{V}_x^{(\alpha)^{\mathrm{T}}} \\ \mathbf{V}_y^{(\alpha)^{\mathrm{T}}} \\ \mathbf{0}^{\mathrm{T}} \end{bmatrix} \quad (\alpha = i, j) \tag{30a}$$

$$\mathbf{L}_{a\kappa}^{(\alpha)} = \frac{1}{2h^{(i,j)}}\begin{bmatrix} h^{(\alpha)}\mathbf{V}_{z,x}^{(\alpha)^{\mathrm{T}}} \\ h^{(\alpha)}\mathbf{V}_{z,y}^{(\alpha)^{\mathrm{T}}} \\ (-1)^{\delta_{\alpha j}}\mathbf{V}_z^{(\alpha)^{\mathrm{T}}} \end{bmatrix} \quad (\alpha = i, j) \tag{30b}$$

3.3. Stress–strain relations

The eccentrically placed adherends in bonded lap joints under uniaxial in-plane external loads result in not only in-plane stresses but also in bending moments in the adherends. This secondary bending induces transverse normal (peeling) stresses in the adhesive. The in-plane stress resultants and bending moments generated by the applied external loading in the adherends are related to the in-plane strain resultants and curvatures, which are defined on the mid-surfaces of the adherends through the constitutive relation as

$$\begin{Bmatrix} \mathbf{N}^{(p)} \\ \mathbf{M}^{(p)} \end{Bmatrix} = \begin{bmatrix} \mathbf{A}^{(p)}(x,y) & \mathbf{B}^{(p)}(x,y) \\ \mathbf{B}^{(p)}(x,y) & \mathbf{D}^{(p)}(x,y) \end{bmatrix} \begin{Bmatrix} \boldsymbol{\varepsilon}^{(p)} \\ \boldsymbol{\kappa}^{(p)} \end{Bmatrix} \tag{31}$$

where

$$\begin{aligned} A_{mn}^{(p)}(x,y) &= h^{(p)}(x,y)\sum_{k=1}^{N_p}(\zeta_{k+1}^{(p)} - \zeta_k^{(p)})\overline{Q}_{mn(k)}^{(p)} \\ B_{mn}^{(p)}(x,y) &= \tfrac{1}{2}(h^{(p)}(x,y))^2\sum_{k=1}^{N_p}(\zeta_{k+1}^{(p)^2} - \zeta_k^{(p)^2})\overline{Q}_{mn(k)}^{(p)} \quad (p = 1, \ldots, P) \\ D_{mn}^{(p)}(x,y) &= \tfrac{1}{3}(h^{(p)}(x,y))^3\sum_{k=1}^{N_p}(\zeta_{k+1}^{(p)^3} - \zeta_k^{(p)^2})\overline{Q}_{mn(k)}^{(p)} \end{aligned} \tag{32}$$

with

$$\zeta_k^{(p)} = \frac{z_k(x,y) - z^{(p)}}{h^{(p)}(x,y)} \quad (k = 1, \ldots, N_p;\ z^{(p)} - h^{(p)} \leqslant z_k \leqslant z^{(p)} + h^{(p)}) \tag{33}$$

In Eq. (31), the matrices $\mathbf{A}^{(p)}$, $\mathbf{D}^{(p)}$, and $\mathbf{B}^{(p)}$, with $(p = 1, \ldots, P)$, are associated with in-plane, bending, and coupled in-plane and bending behaviors of the adherends, and $\overline{Q}_{mn(k)}^{(p)}$ $(p = 1, \ldots, P)$ are the

coefficients of the reduced stiffness matrix of the kth ply defined in the global $(x-y)$ coordinate system. Note that the tapered adherend thickness, $2h^{(p)}(p=1,\ldots,P)$, varies as a function of the global $(x-y)$ coordinates. Hence, the material property matrices associated with the adherends, $\mathbf{A}^{(p)}$, $\mathbf{D}^{(p)}$, and $\mathbf{B}^{(p)}$, are dependent on the in-plane coordinates.

Furthermore, the ratio of the ply thickness to the adherend thickness is assumed to be constant, i.e., $t_k^{(p)}(x,y)/2h^{(p)}(x,y)=\bar{t}_k^{(p)}=$ constant. In this case, the material property matrices, $\mathbf{A}^{(p)}$, $\mathbf{D}^{(p)}$, and $\mathbf{B}^{(p)}$, become dependent only on the adherend thickness, $2h^{(p)}(x,y)$, with $(p=1,\ldots,P)$.

The relation given in Eq. (31) can be compacted in the form

$$\mathbf{s}^{(p)}=\mathbf{E}^{(p)}\mathbf{e}^{(p)}\quad(p=1,\ldots,P) \tag{34}$$

in which $\mathbf{s}^{(p)}$, $\mathbf{E}^{(p)}$, and $\mathbf{e}^{(p)}$ are defined as

$$\mathbf{s}^{(p)^{\mathrm{T}}}=\left\{\mathbf{N}^{(p)^{\mathrm{T}}},\mathbf{M}^{(p)^{\mathrm{T}}}\right\} \tag{35a}$$

$$\mathbf{E}^{(p)}=\begin{bmatrix}\mathbf{A}^{(p)} & \mathbf{B}^{(p)}\\ \mathbf{B}^{(p)} & \mathbf{D}^{(p)}\end{bmatrix} \tag{35b}$$

$$\mathbf{e}^{(p)^{\mathrm{T}}}=\left\{\boldsymbol{\varepsilon}^{(p)^{\mathrm{T}}},\boldsymbol{\kappa}^{(p)^{\mathrm{T}}}\right\} \tag{35c}$$

With the representation of $\mathbf{e}^{(p)}$ in Eq. (24), the stress–strain relations given in Eq. (35) can be rewritten as

$$\mathbf{s}^{(p)}=\mathbf{E}^{(p)}\mathbf{H}^{(p)}(\mathbf{q}^{(p)})\mathbf{q}^{(p)}\quad(p=1,\ldots,P) \tag{36}$$

Because the adhesives do not sustain in-plane deformation, the in-plane stress components, $\sigma_{xx}^{(i,j)}$, $\sigma_{yy}^{(i,j)}$, and $\sigma_{xy}^{(i,j)}$, are disregarded. In the adhesive between the ith and jth adherends, the transverse shear stresses, $\sigma_{xz}^{(i,j)}$ and $\sigma_{yz}^{(i,j)}$, and the transverse normal stress, $\sigma_{zz}^{(i,j)}$, are related to the corresponding strain components through a bilinear relation as

$$\mathbf{s}^{(i,j)}=\mathbf{E}^{(i,j)}\boldsymbol{\varepsilon}^{(i,j)} \tag{37}$$

where

$$\mathbf{s}^{(i,j)^{\mathrm{T}}}=h^{(i,j)}\left\{\sigma_{xz}^{(i,j)},\sigma_{yz}^{(i,j)},\sigma_{zz}^{(i,j)}\right\} \tag{38a}$$

$$\boldsymbol{\varepsilon}^{(i,j)^{\mathrm{T}}}=\left\{\gamma_{xz}^{(i,j)},\gamma_{yz}^{(i,j)},\varepsilon_{zz}^{(i,j)}\right\} \tag{38b}$$

$$\mathbf{E}^{(i,j)}\left(\mathbf{q}^{(i)},\mathbf{q}^{(j)}\right)=\begin{bmatrix}G_{\mathrm{eff}}^{(i,j)}(\mathbf{q}^{(i)},\mathbf{q}^{(j)}) & 0 & 0\\ 0 & G_{\mathrm{eff}}^{(i,j)}(\mathbf{q}^{(i)},\mathbf{q}^{(j)}) & 0\\ 0 & 0 & E_{\mathrm{eff}}^{(i,j)}(\mathbf{q}^{(i)},\mathbf{q}^{(j)})\end{bmatrix} \tag{38c}$$

in which the expressions for $G_{\mathrm{eff}}^{(i,j)}(\mathbf{q}^{(i)},\mathbf{q}^{(j)})=G_{\mathrm{eff}}^{(i,j)}(\gamma_{\mathrm{eff}}^{(i,j)})$ and $E_{\mathrm{eff}}^{(i,j)}(\mathbf{q}^{(i)},\mathbf{q}^{(j)})=E_{\mathrm{eff}}^{(i,j)}(\gamma_{\mathrm{eff}}^{(i,j)})$ are defined in Eqs. (5) and (7), respectively.

Substituting for the expression for $\boldsymbol{\varepsilon}^{(i,j)}$ from Eq. (27) permits the stress–strain relations given in Eq. (38) to be expressed in terms of the unknowns of the adherends as

$$\mathbf{s}^{(i,j)}=\mathbf{E}^{(i,j)}(\mathbf{q}^{(i)},\mathbf{q}^{(j)})(\mathbf{L}_a^{(i)}\mathbf{q}^{(i)}-\mathbf{L}_a^{(j)}\mathbf{q}^{(j)}) \tag{39}$$

3.4. Boundary conditions

Along the mth segment of the boundary of the adherends, denoted by $\Gamma_m^{(p)}$, with $(p=1,\ldots,P)$, as shown in Fig. 1, the prescribed displacement components normal and tangent to the boundary, ${}_{(m)}\hat{u}_n^{(p)}$, ${}_{(m)}\hat{u}_t^{(p)}$, and ${}_{(m)}\hat{u}_z^{(p)}$, and the slope normal to the boundary, ${}_{(m)}\hat{u}_{z,n}^{(p)}$, can be imposed as

$$\begin{aligned} u_n^{(p)} &= {}_{(m)}\hat{u}_n^{(p)} \\ u_t^{(p)} &= {}_{(m)}\hat{u}_t^{(p)} \\ u_z^{(p)} &= {}_{(m)}\hat{u}_z^{(p)} \\ u_{z,n}^{(p)} &= {}_{(m)}\hat{u}_{z,n}^{(p)} \end{aligned} \quad \text{on} \quad \Gamma_m^{(p)} (p = 1, \ldots, P; m = 1, 2, 3, 4) \tag{40}$$

Utilizing the vector representations of the displacement components given by Eq. (10), these prescribed displacements can be expressed in vector form as

$$\mathbf{V}_m^{(p)^{\mathrm{T}}} \mathbf{q}^{(p)} - \hat{\mathbf{u}}_m^{(p)} = \mathbf{0} \quad (p = 1, \ldots, P; m = 1, 2, 3, 4) \tag{41}$$

where the matrix $\mathbf{V}_m^{(p)}$ and the vector $\hat{\mathbf{u}}_m^{(p)}$ are defined as

$$\mathbf{V}_m^{(p)^{\mathrm{T}}} = \left[(\mathbf{n}_m^{(p)^{\mathrm{T}}} \mathbf{e}_1) \mathbf{V}_x^{(p)^{\mathrm{T}}} + (\mathbf{n}_m^{(p)^{\mathrm{T}}} \mathbf{e}_2) \mathbf{V}_y^{(p)^{\mathrm{T}}} - (\mathbf{n}_m^{(p)^{\mathrm{T}}} \mathbf{e}_2) \mathbf{V}_x^{(p)^{\mathrm{T}}} + (\mathbf{n}_m^{(p)^{\mathrm{T}}} \mathbf{e}_1) \mathbf{V}_y^{(p)^{\mathrm{T}}} \mathbf{V}_z^{(p)^{\mathrm{T}}} (\mathbf{n}_m^{(p)^{\mathrm{T}}} \mathbf{e}_1) \mathbf{V}_{z,x}^{(p)^{\mathrm{T}}} + (\mathbf{n}_m^{(p)^{\mathrm{T}}} \mathbf{e}_1) \mathbf{V}_{z,y}^{(p)^{\mathrm{T}}} \right] \tag{42}$$

and

$$\hat{\mathbf{u}}_m^{(p)^{\mathrm{T}}} = \left\{ {}_{(m)}\hat{u}_n^{(p)} \quad {}_{(m)}\hat{u}_t^{(p)} \quad {}_{(m)}\hat{u}_z^{(p)} \quad {}_{(m)}\hat{u}_{z,n}^{(p)} \right\} \tag{43}$$

with $\mathbf{e}_1$ and $\mathbf{e}_2$ being the base vectors of the global coordinates.

The boundary conditions in Eq. (41) are enforced as constraint conditions by introducing Lagrange multiplier functions, $\Lambda_{\alpha m}^{(p)}(t)$, with $\alpha = n, t, z$, and $\Lambda_{zm}^{\prime(p)}(t)$, defined along the mth boundary segment. These boundary conditions are written in integral form as

$$\int_{\Gamma_m^{(p)}} \mathbf{\Lambda}_m^{(p)}(t) \left\{ \mathbf{V}_m^{(p)T} \mathbf{q}^{(p)} - \hat{\mathbf{u}}_m^{(p)} \right\} dt = 0 \quad (p = 1, \ldots, P; m = 1, 2, 3, 4) \tag{44}$$

where the matrix $\mathbf{\Lambda}_m^{(p)}$ contains the Lagrange multiplier functions in the form

$$\mathbf{\Lambda}_m^{(p)}(t) = \begin{bmatrix} \Lambda_{nm}^{(p)}(t) & & & \\ & \Lambda_{tm}^{(p)}(t) & & \\ & & \Lambda_{zm}^{(p)}(t) & \\ & & & \Lambda_{zm}^{\prime(p)}(t) \end{bmatrix} \quad (p = 1, \ldots, P; m = 1, 2, 3, 4) \tag{45}$$

where the unknown Lagrange multiplier functions, $\Lambda_{\alpha m}^{(p)}(t)$, with $\alpha = n, t, z$, and $\Lambda_{zm}^{\prime(p)}(t)$, are assumed in polynomial forms as

$$\left(\Lambda_{\alpha m}^{(p)}(t(\xi)), \Lambda_{zm}^{\prime(p)}(t(\xi)) \right) = \sum_{s=0}^{S} \left(\lambda_{s(\alpha m)}^{(p)}, \lambda_{s(zm)}^{\prime(p)} \right) T_s(\xi; \mathbf{t}_{\Gamma_m}^{(p)}, K) \quad (p = 1, \ldots, P; m = 1, 2, 3, 4) \tag{46}$$

where $T_s(\xi; \mathbf{t}_{\Gamma_m}^{(p)}, K)$ represents the sth term of the $(K-1)$th-degree B-spline functions defined along the straight boundary segment $\Gamma_m^{(p)}$, with $\mathbf{t}_{\Gamma_m}^{(p)}$ being the associated knot vector. Also, $\lambda_{s(\alpha m)}$ and $\lambda'_{s(zm)}$, with $\alpha = n, t, z$, are the unknown Lagrange multipliers associated with the B-spline functions, $T_s(\xi; \mathbf{t}_{\Gamma_m}^{(p)}, K)$.

Substituting the expressions for the Lagrange multiplier functions from Eq. (46) into Eq. (45) and rearranging the terms, the constraint equations representing the prescribed displacements can be rewritten as

$$\boldsymbol{\lambda}_m^{(p)^{\mathrm{T}}} (\mathbf{C}_m^{(p)} \mathbf{q}^{(p)} - \mathbf{f}_{mc}^{(p)}) = 0 \tag{47}$$

where

$$\boldsymbol{\lambda}_m^{(p)^{\mathrm{T}}} = \left\{ \boldsymbol{\lambda}_{1m}^{(p)^{\mathrm{T}}}, \quad \boldsymbol{\lambda}_{2m}^{(p)^{\mathrm{T}}}, \quad \cdots, \quad \boldsymbol{\lambda}_{Sm}^{(p)^{\mathrm{T}}} \right\} \tag{48}$$

with

$$\boldsymbol{\lambda}_{km}^{(p)^{\mathrm{T}}} = \left\{ \lambda_{k(nm)}^{(p)}, \quad \lambda_{k(tm)}^{(p)}, \quad \lambda_{k(zm)}^{(p)}, \quad \lambda_{k(zm)}^{\prime(p)} \right\} \tag{49}$$

and

$$\mathbf{C}_{m}^{(p)^{\mathrm{T}}} = \left[\mathbf{C}_{1m}^{(p)^{\mathrm{T}}} \quad \mathbf{C}_{2m}^{(p)^{\mathrm{T}}} \quad \cdots \quad \mathbf{C}_{Sm}^{(p)^{\mathrm{T}}} \right] \tag{50}$$

with

$$\mathbf{C}_{sm}^{(p)} = \int_{\Gamma_m^{(p)}} T_s(\xi; \mathbf{t}_{\Gamma_m}^{(p)}, K) \mathbf{V}_m^{(p)^{\mathrm{T}}} \, \mathrm{d}\Gamma \tag{51}$$

and

$$\mathbf{f}_{mc}^{(p)^{\mathrm{T}}} = \left\{ \mathbf{f}_{1(mc)}^{(p)^{\mathrm{T}}}, \quad \mathbf{f}_{2(mc)}^{(p)^{\mathrm{T}}}, \quad \cdots, \quad \mathbf{f}_{S(mc)}^{(p)^{\mathrm{T}}} \right\} \tag{52}$$

with

$$\mathbf{f}_{s(mc)}^{(p)^{\mathrm{T}}} = \int_{\Gamma_m^{(p)}} T_s(\xi; \mathbf{t}_{\Gamma_m}^{(p)}, K) \hat{\mathbf{u}}_m^{(p)^{\mathrm{T}}} \, \mathrm{d}\Gamma \tag{53}$$

for ($p = 1, \ldots, P$; $m = 1, 2, 3, 4$).

The constraint equations in Eq. (47) can be assembled to form a single matrix equation combining all of the constraint equations as

$$\boldsymbol{\lambda}^{(p)^{\mathrm{T}}} (\mathbf{C}^{(p)} \mathbf{q}^{(p)} - \mathbf{f}_c^{(p)}) = 0 \quad (p = 1, \ldots, P) \tag{54}$$

where

$$\boldsymbol{\lambda}^{(p)^{\mathrm{T}}} = \left\{ \boldsymbol{\lambda}_1^{(p)^{\mathrm{T}}}, \quad \boldsymbol{\lambda}_2^{(p)^{\mathrm{T}}}, \quad \boldsymbol{\lambda}_3^{(p)^{\mathrm{T}}}, \quad \boldsymbol{\lambda}_4^{(p)^{\mathrm{T}}} \right\} \tag{55a}$$

$$\mathbf{C}^{(p)^{\mathrm{T}}} = \left[\mathbf{C}_1^{(p)^{\mathrm{T}}} \quad \mathbf{C}_2^{(p)^{\mathrm{T}}} \quad \mathbf{C}_3^{(p)^{\mathrm{T}}} \quad \mathbf{C}_4^{(p)^{\mathrm{T}}} \right] \tag{55b}$$

$$\mathbf{f}_c^{(p)^{\mathrm{T}}} = \left\{ \mathbf{f}_{1c}^{(p)^{\mathrm{T}}}, \quad \mathbf{f}_{2c}^{(p)^{\mathrm{T}}}, \quad \mathbf{f}_{3c}^{(p)^{\mathrm{T}}}, \quad \mathbf{f}_{4c}^{(p)^{\mathrm{T}}} \right\} \tag{55c}$$

The constraint equations in Eq. (54) are linearly independent, provided the rank of the matrix $\mathbf{C}^{(p)}$ is equal to the total number of constraint equations. Also, Eq. (54) can be treated as the potential energy of the reaction forces producing zero energy since $\mathbf{C}^{(p)} \mathbf{q}^{(p)} = \mathbf{0}$, and it can be referred to as the potential energy of the constraint forces, V_c, in the form

$$V_c = \sum_{p=1}^{p} \boldsymbol{\lambda}^{(p)^{\mathrm{T}}} \left(\mathbf{C}^{(p)} \mathbf{q}^{(p)} - \mathbf{f}_c^{(p)} \right) = 0 \tag{56}$$

3.5. Governing equations

The governing equations are derived based on the principle of virtual work

$$\delta W_{\mathrm{int}} = \delta W_{\mathrm{ext}} \tag{57}$$

where δW_{int} and δW_{ext} represent the virtual work due to internal and external forces, respectively, of the bonded lap joint. The internal virtual work, δW_{int}, is the sum of the internal virtual work of the adherends and the adhesives, i.e.,

$$\delta W_{\text{int}} = \sum_{p=1}^{P} \delta W_{\text{int}}^{(p)} + \sum_{i=1}^{P} \sum_{j=i+1}^{P} a^{(i,j)} \delta W_{\text{int}}^{(i,j)} \tag{58}$$

where the internal virtual work in the adherends and adhesives are expressed as

$$\delta W_{\text{int}}^{(p)} = \int_{A^{(p)}} \delta \mathbf{e}^{(p)^{\mathrm{T}}} \mathbf{s}^{(p)} \mathrm{d}A = \int_{A^{(p)}} \delta \mathbf{e}^{(p)^{\mathrm{T}}} \mathbf{E}^{(p)} \mathbf{e}^{(p)} \mathrm{d}A \tag{59}$$

$$\delta W_{\text{int}}^{(i,j)} = \int_{A^{(i,j)}} \delta \boldsymbol{\varepsilon}^{(i,j)^{\mathrm{T}}} \mathbf{s}^{(i,j)} \mathrm{d}A = \int_{A^{(i,j)}} \delta \boldsymbol{\varepsilon}^{(i,j)^{\mathrm{T}}} \mathbf{E}^{(i,j)} \boldsymbol{\varepsilon}^{(i,j)} \mathrm{d}A \tag{60}$$

The term $a^{(i,j)}$ is used to designate the presence of adhesive bonding and the consistency of stacking order between adherends i and j, i.e., the elevation of adherend i is always higher that of adherend j. Hence, the term $a^{(i,j)}$ is defined as

$$a^{(i,j)} = \begin{cases} 1 \text{ adhesive between adherends } i \text{ and } j, \text{ and } z^{(i)} > z^{(j)} \\ 0 \text{ no adhesive between adherends } i \text{ and } j, \text{ or } z^{(i)} < z^{(j)} \end{cases}$$

Substituting from Eqs. (24) and (27) and with the special property of $\delta[\mathbf{L}_N^{(p)}(\mathbf{q}^{(p)})]\mathbf{q}^{(p)} = 2\mathbf{L}_N^{(p)}(\mathbf{q}^{(p)})\delta\mathbf{q}^{(p)}$, the total virtual strain vectors, $\delta\boldsymbol{\varepsilon}^{(i,j)}$ and $\delta\mathbf{e}^{(p)}$, are obtained as

$$\delta \boldsymbol{\varepsilon}^{(i,j)} = \mathbf{L}_a^{(i)} \delta \mathbf{q}^{(i)} - \mathbf{L}_a^{(j)} \delta \mathbf{q}^{(j)} \tag{61}$$

and

$$\delta \mathbf{e}^{(p)} = \left[\mathbf{L}_L^{(p)} + 2\mathbf{L}_N^{(p)}(\mathbf{q}^{(p)}) \right] \delta \mathbf{q}^{(p)} = {}^{*}\mathbf{H}^{(p)}(\mathbf{q}^{(p)}) \delta \mathbf{q}^{(p)} \tag{62a}$$

where

$${}^{*}\mathbf{H}^{(p)}(\mathbf{q}^{(p)}) = \mathbf{L}_L^{(p)} + 2\mathbf{L}_N^{(p)}(\mathbf{q}^{(p)}) \tag{62b}$$

with $(p = 1, \ldots, P)$. The external virtual work is expressed as the sum of the virtual work due to externally applied forces, $\delta W_{\text{ext}}^{(p)}$, and that arising from the boundary reaction forces, $\delta W_c^{(p)}$, i.e.,

$$\delta W_{\text{ext}} = \sum_{p=1}^{P} \delta W_{\text{ext}}^{(p)} + \delta W_c^{(p)} \tag{63}$$

The virtual work due to externally applied forces, $\delta W_{\text{ext}}^{(p)}$, can be expressed in matrix notation as

$$\delta W_{\text{ext}}^{(p)} = \delta \mathbf{q}^{(p)T} \mathbf{p}^{(p)} \tag{64}$$

in which

$$\mathbf{p}^{(p)T} = \left\{ \mathbf{p}_{\varepsilon}^{(p)T}, \mathbf{p}_{\kappa}^{(p)T} \right\} \tag{65}$$

with

$$\mathbf{p}_{\varepsilon}^{(p)} = \int_{\Gamma^{(p)}} \left\{ \mathbf{V}_x^{(p)} t_x + \mathbf{V}_y^{(p)} t_y \right\} \mathrm{d}\Gamma \tag{66a}$$

$$\mathbf{p}_{\kappa}^{(p)} = \int_{\Gamma^{(p)}} \left\{ \mathbf{V}_z^{(p)} p_z + \mathbf{V}_{z,x}^{(p)} m_x + \mathbf{V}_{z,y}^{(p)} m_y \right\} \mathrm{d}\Gamma \tag{66b}$$

The virtual work due to the boundary reaction forces, $\delta W_c^{(p)}$, is identical to the first variation of the potential energy expression in Eq. (56) as

$$\begin{aligned} \delta W_c^{(p)} &= -\delta V_c^{(p)} \\ &= -\delta \boldsymbol{\lambda}^{(p)^{\mathrm{T}}} (\mathbf{C}^{(p)} \mathbf{q}^{(p)} - \mathbf{f}_c^{(p)}) - \delta \mathbf{q}^{(p)^{\mathrm{T}}} \mathbf{C}^{(p)^{\mathrm{T}}} \boldsymbol{\lambda}^{(p)} \end{aligned} \tag{67}$$

The virtual work due to the boundary reactions (constraint conditions) can be interpreted as the virtual work of the constraint forces, $\boldsymbol{\lambda}^{(p)}$, over the virtual displacements, $\delta(\mathbf{C}^{(p)}\mathbf{q}^{(p)})$, of the adherends and the virtual work of the constrained displacements (boundary conditions), $\mathbf{C}^{(p)}\mathbf{q}^{(p)} - \mathbf{f}_c^{(p)}$, over the virtual constraint forces, $\delta\boldsymbol{\lambda}^{(p)}$. Although the term inside the parentheses in Eq. (67) is identical to zero, it is included in the virtual work expression in order to obtain a complete set of equations that contains both equilibrium equations and constraint conditions (kinematic boundary conditions) along the boundary of the adherends.

Substituting from Eqs. (59), (60), (64) and (67) while invoking the strain vectors, $\mathbf{e}^{(p)}(p = 1,\ldots,P)$ and $\boldsymbol{\varepsilon}^{(i,j)}$, from Eqs. (24) and (27), and their virtual forms, $\delta\mathbf{e}^{(p)}(p = 1,\ldots,r)$ and $\delta\boldsymbol{\varepsilon}^{(i,j)}$, from Eqs. (61) and (62), and rearranging the terms, the virtual work expression of Eq. (57) can be rewritten as

$$\begin{aligned}
&\sum_{p=1}^{P} \delta\mathbf{q}^{(p)^{\mathrm{T}}}(\mathbf{K}^{(p)}(\mathbf{q}^{(p)}))\mathbf{q}^{(p)} + \sum_{i=1}^{P}\sum_{\substack{j=1\\ j\neq i}}^{P}\Big\{\delta\mathbf{q}^{(i)^{\mathrm{T}}}(\mathbf{K}_{ii}^{(i,j)}(\mathbf{q}^{(i)},\mathbf{q}^{(j)}))\mathbf{q}^{(i)} \\
&-\delta\mathbf{q}^{(i)^{\mathrm{T}}}\mathbf{K}_{ij}^{(i,j)}(\mathbf{q}^{(i)},\mathbf{q}^{(j)})\mathbf{q}^{(j)} - \delta\mathbf{q}^{(j)^{\mathrm{T}}}\mathbf{K}_{ji}^{(i,j)}(\mathbf{q}^{(i)},\mathbf{q}^{(j)})\mathbf{q}^{(i)} + \delta\mathbf{q}^{(j)^{\mathrm{T}}}\Big(\mathbf{K}_{jj}^{(i,j)}(\mathbf{q}^{(i)},\mathbf{q}^{(j)})\Big)\mathbf{q}^{(j)}\Big\} \\
&= \sum_{p=1}^{P}\delta\mathbf{q}^{(p)^{\mathrm{T}}}\mathbf{p}^{(p)} - \delta\boldsymbol{\lambda}^{(p)^{\mathrm{T}}}\mathbf{C}^{(p)}\mathbf{q}^{(p)} - \delta\mathbf{q}^{(p)^{\mathrm{T}}}\mathbf{C}^{(p)^{\mathrm{T}}}\boldsymbol{\lambda}^{(p)} + \delta\boldsymbol{\lambda}^{(p)^{\mathrm{T}}}\mathbf{f}_c^{(p)}
\end{aligned} \tag{68}$$

where

$$\mathbf{K}^{(p)}(\mathbf{q}^{(p)}) = \int_{A_p} {}^{*}\mathbf{H}^{(p)^{\mathrm{T}}}(\mathbf{q}^{(p)})\mathbf{E}^{(p)}\mathbf{H}^{(p)}(\mathbf{q}^{(p)})\mathrm{d}A \quad (p = 1,\ldots,P) \tag{69a}$$

$$\mathbf{K}_{\alpha\beta}^{(i,j)}(\mathbf{q}^{(i)},\mathbf{q}^{(j)}) = a^{(i,j)}\int_{A^{(i,j)}} \mathbf{L}_a^{(\alpha)^{\mathrm{T}}}\mathbf{E}^{(i,j)}(\mathbf{q}^{(i)},\mathbf{q}^{(j)})\mathbf{L}^{(\beta)}\mathrm{d}A \quad (\alpha,\beta = i,j) \tag{69b}$$

For arbitrary variations of the virtual solution vectors $\delta\mathbf{q}^{(p)}$ and $\delta\boldsymbol{\lambda}^{(p)}$ $(p = 1,\ldots,P)$, Eq. (68) can further be rearranged and put into a more compact form

$$\begin{bmatrix}
\mathbf{K}_{11} & \mathbf{K}_{12} & \ldots & \mathbf{K}_{1P} & \mathbf{C}^{(1)^{\mathrm{T}}} & \mathbf{0} & \cdots & \mathbf{0} \\
\mathbf{K}_{12}^{\mathrm{T}} & \mathbf{K}_{22} & \ldots & \mathbf{K}_{2P} & \mathbf{0} & \mathbf{C}^{(2)^{\mathrm{T}}} & \cdots & \mathbf{0} \\
\vdots & \vdots & \vdots & \vdots & \vdots & \vdots & \vdots & \vdots \\
\mathbf{K}_{1P}^{\mathrm{T}} & \mathbf{K}_{2P}^{\mathrm{T}} & \cdots & \mathbf{K}_{PP} & \mathbf{0} & \mathbf{0} & \mathbf{0} & \mathbf{C}^{(P)^{\mathrm{T}}} \\
\mathbf{C}^{(1)} & \mathbf{0} & \cdots & \mathbf{0} & \mathbf{0} & \mathbf{0} & \cdots & \mathbf{0} \\
\mathbf{0} & \mathbf{C}^{(2)} & \cdots & \mathbf{0} & \mathbf{0} & \mathbf{0} & \cdots & \mathbf{0} \\
\vdots & \vdots & \vdots & \vdots & \vdots & \vdots & \vdots & \vdots \\
\mathbf{0} & \mathbf{0} & \mathbf{0} & \mathbf{C}^{(P)} & \mathbf{0} & \mathbf{0} & \mathbf{0} & \mathbf{0}
\end{bmatrix} \times \begin{Bmatrix} \mathbf{q}^{(1)} \\ \mathbf{q}^{(2)} \\ \vdots \\ \mathbf{q}^{(P)} \\ \boldsymbol{\lambda}^{(1)} \\ \boldsymbol{\lambda}^{(2)} \\ \vdots \\ \boldsymbol{\lambda}^{(P)} \end{Bmatrix} = \begin{Bmatrix} \mathbf{p}^{(1)} \\ \mathbf{p}^{(2)} \\ \vdots \\ \mathbf{p}^{(P)} \\ \mathbf{f}_c^{(1)} \\ \mathbf{f}_c^{(2)} \\ \vdots \\ \mathbf{f}_c^{(P)} \end{Bmatrix} \tag{70}$$

where

$$\mathbf{K}_{mn} = \begin{cases} \mathbf{K}^{(m)}(\mathbf{q}^{(m)}) + \sum\limits_{\substack{i=1\\ i\neq m}}^{P}\left(\mathbf{K}_{mm}^{(m,i)}(\mathbf{q}^{(m)},\mathbf{q}^{(i)}) + \mathbf{K}_{mm}^{(i,m)}(\mathbf{q}^{(i)},\mathbf{q}^{(m)})\right) \text{ if}(m = n) \\ -\left(\mathbf{K}_{mn}^{(m,n)}\left(\mathbf{q}^{(\mathrm{m})},\mathbf{q}^{(n)}\right) + \mathbf{K}_{mn}^{(n,m)}(\mathbf{q}^{(\mathrm{n})},\mathbf{q}^{(m)})\right) \text{ if}(m \neq n) \end{cases}$$

and

$$\mathbf{K}_{mn} = \mathbf{K}_{nm}^{\mathrm{T}} \text{ if}(m \neq n) \tag{71}$$

Note that the submatrices of the stiffness matrix are dependent on the unknown variables, rendering the governing equations nonlinear, and that these submatrices are non-symmetric. The solution to this equation requires a nonlinear iterative solution technique that utilizes **LU** decomposition because sub-matrices $\mathbf{K}_{ii}$ on the diagonal are nonsymmetric. Therefore, the Newton–Raphson iteration method in conjunction

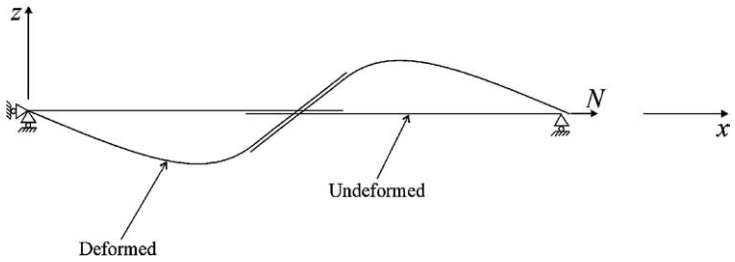

Fig. 5. The scaled deformation of the bonded lap joint made of isotropic adherends with linear adhesive behavior at the last load step ($N/N_0 = 1$).

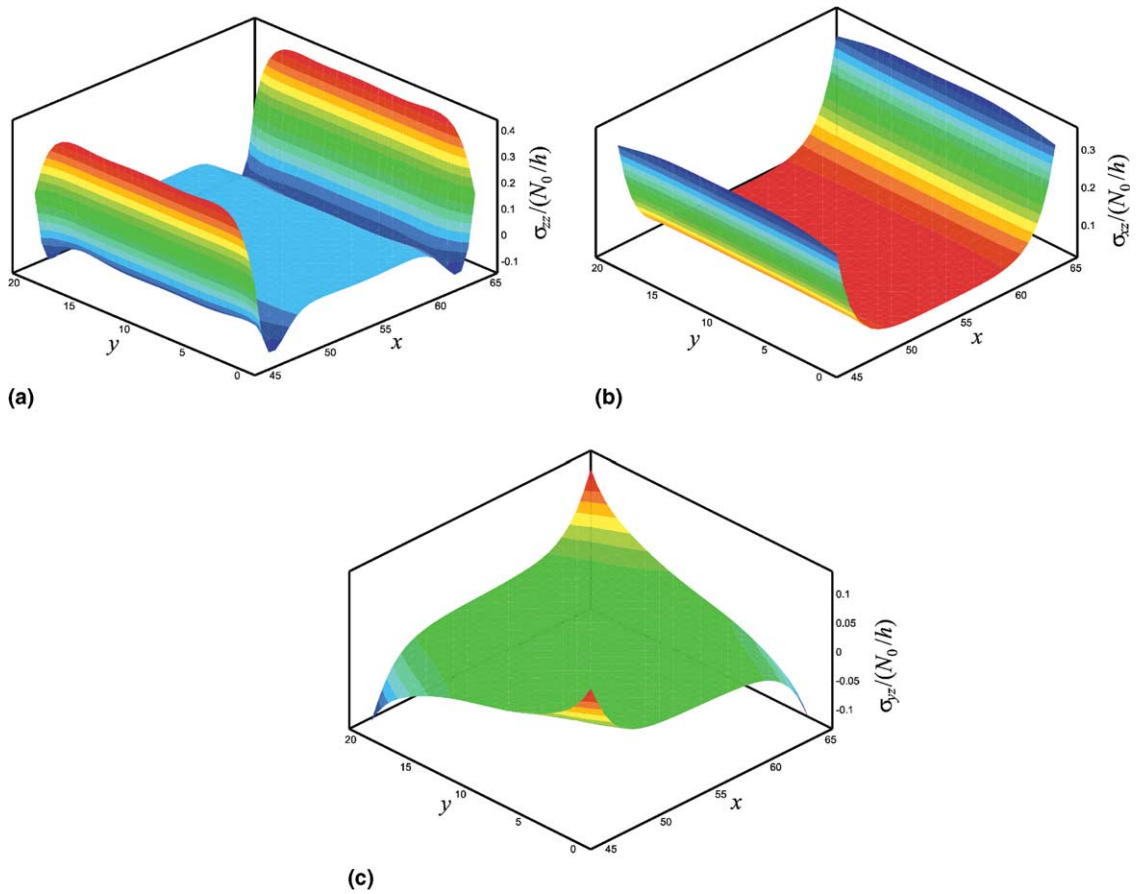

Fig. 6. Variation of the stress components in the adhesive: (a) peeling stress, σ_{zz}; (b) shearing stress, σ_{xz}; and (c) shearing stress, σ_{yz} with linear adhesive behavior.

with Broyden's automatic Jacobian matrix update procedure is employed. The iterative solution procedure described in detail in Appendix B begins with the initial guess of the incremental unknown variables. The initial guess is obtained from the linearized equilibrium equations, and the converged solution is achieved through incremental corrections to the initial guess.

4. Numerical results

The present approach is first validated against the nonlinear finite element solution of isotropic single-lap joint with linear and bilinear adhesive behaviors. As described in Fig. 4a, the adherends have identical planar geometries, with the width and length dimensions specified as $W^{(p)} = 20$ mm, $L^{(p)} = 60$ mm, and $\Delta^{(p)} = 0$ with $p = 1,2$. The overlap (adhesive) length of the joint is given as $L^{(1,2)} = 20$ mm. The thicknesses of the adherends and the adhesive are specified as $2h^{(p)} = 1.5$ mm and $2h^{(1,2)} = 0.2$ mm, respectively. These dimensions are the same as those considered previously by Edlund and Klarbring (1992).

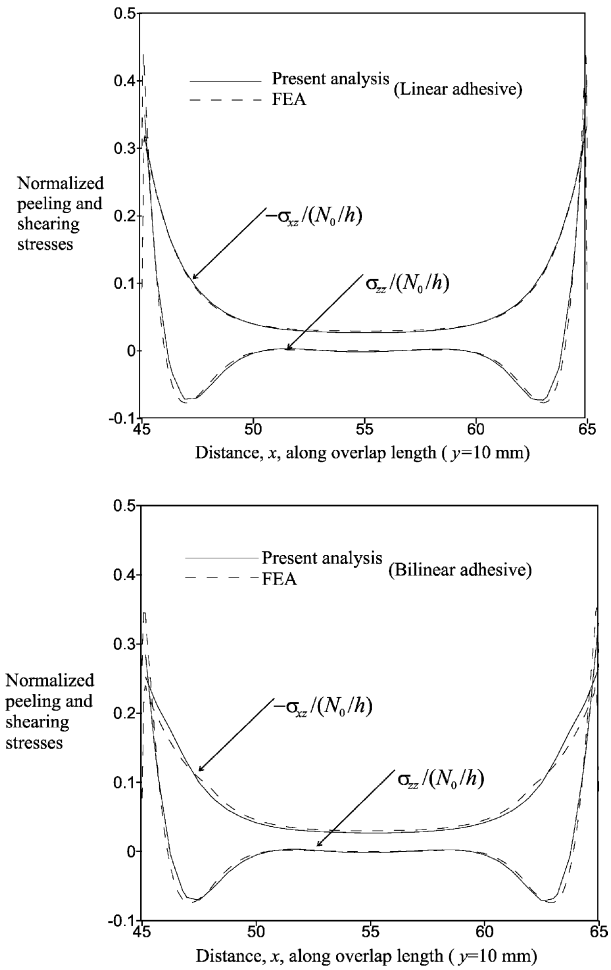

Fig. 7. Comparison of the peeling stress, σ_{zz}, and shearing stress, σ_{xz}, along the horizontal centerline, between the present approach and the finite element analysis: linearly adhesive and bilinear adhesive behavior.

The adherends are made of aluminum with Young's modulus and Poisson's ratio specified as $E^{(p)} = 70$ GPa and $v^{(p)} = 0.3$, respectively. Also, the adhesive exhibits either a linear or a bilinear elastic material behavior. In the case of linearly elastic material behavior, the shear modulus and Poisson's ratio of the adhesive are specified as $G^{(1,2)} = 3$ GPa and $v^{(1,2)} = 0.3$, respectively. In the case of bilinear material behavior, the material parameters of the adhesive are defined as $G_1^{(1,2)} = 3$ GPa, $G_2^{(1,2)} = 1.5$ GPa, and $v^{(1,2)} = 0.3$. The single-lap joint simply supported along the loaded ends is subjected to uniform tension of $N_0 = 150$ N/mm in 10 equal load increments.

Prior to establishing the validity of present approach, a convergence study was performed to establish the optimum number of knot points. Starting with the initial knot point numbers of $N_x^{(p)} = 11$ and $N_y^{(p)} = 7$, which respectively correspond to the number of terms of $M_x^{(p)} = 9$ and $M_y^{(p)} = 5$, they were gradually incremented in the longitudinal direction. The final values of $N_x^{(p)} = 21$ and $N_y^{(p)} = 7$, which produce $M_x^{(p)} = 19$ and $M_y^{(p)} = 5$ terms in the series representation in the x- and y-directions, respectively ensure convergence within 1% difference between two consecutive analyses. These values result in a total of 798 unknown generalized coordinates in this analysis. The coordinates of the knot vectors employed for each adherend are given as

$$\mathbf{t}_x^{(1)^{\mathrm{T}}} = \{45, 46, 47, 49, 52, 55, 58, 61, 63, 64, 64.5, 65, 66, 69, 74, 80, 87.5, 95, 101, 106, 110\}$$

$$\mathbf{t}_x^{(2)^{\mathrm{T}}} = \{0, 4, 9, 15, 22.5, 30, 36, 41, 44, 45, 46, 47, 49, 52, 55, 58, 61, 63, 64, 64.5, 65\}$$

$$\mathbf{t}_y^{(1)} = \mathbf{t}_y^{(2)} = \{0, 3.33, 6.66, 10, 13.33, 16.66, 20\}$$

Note that the spacing between the knot points is unequal in the longitudinal direction. In order to capture the edge effects on the stress concentration in the adhesive, the knot points in the longitudinal direction are closely spaced near the adhesive edges whereas the spacing is larger away from the adhesive edges.

The present analysis results are compared against predictions obtained from a two-dimensional nonlinear finite element analysis (FEA) using ANSYS, a commercially available program. For the FEA under plane stress assumptions, the adherends and adhesive were discretized, respectively, by 16 and 6 layers of quadrilateral elements through the thickness leading to a total of 7648 elements and 8011 nodes. The scaled deformation of the bonded single-lap joint with linearly elastic adhesive behavior at the final load step is shown in Fig. 5. As observed in this figure, the bonded single-lap joint bends asymmetrically as it

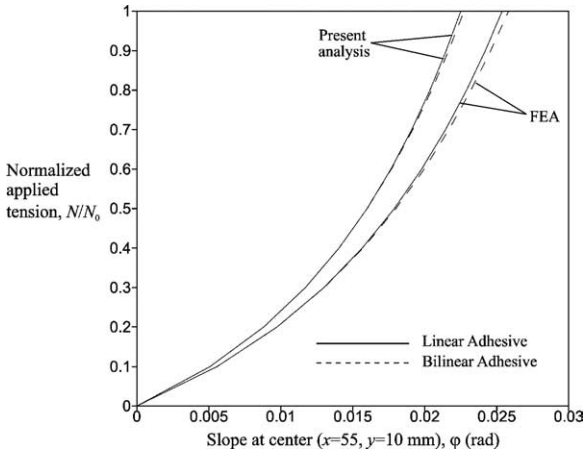

Fig. 8. Comparison of the rotation at the center of the overlap as a function of applied load between the present approach and the finite element analysis.

is stretched from the right edge of the lower adherend. The asymmetric deformation occurs primarily due to the presence of eccentric loading, boundary conditions, and the geometrical coupling between the adherends.

For the case of linearly elastic adhesive material behavior, the transverse normal (peeling), σ_{zz}, and transverse shear stresses, σ_{xz} and σ_{yz}, in the adhesive corresponding to the final load step are illustrated in Fig. 6. The steep variations of the peeling, σ_{zz}, and shearing stresses, σ_{xz} and σ_{yz}, near the edges and corners of the adhesive are successfully captured by the present approach. Note that both the peeling stress σ_{zz} and the shearing stress σ_{xz} are symmetric along the horizontal and vertical centerlines of the adhesive whereas the shearing stress σ_{yz} is asymmetrically distributed.

A comparison of the peeling stress σ_{zz} and the shearing stress σ_{xz} evaluated along the horizontal centerline (i.e., along $y = 10$ mm) from the present analysis with those of the FEA is shown in Fig. 7. The comparison indicates close agreement for both the linearly elastic and bilinear adhesive material behaviors. Although the classical laminate and shear-lag theories adopted for simplifying the modeling of adherends

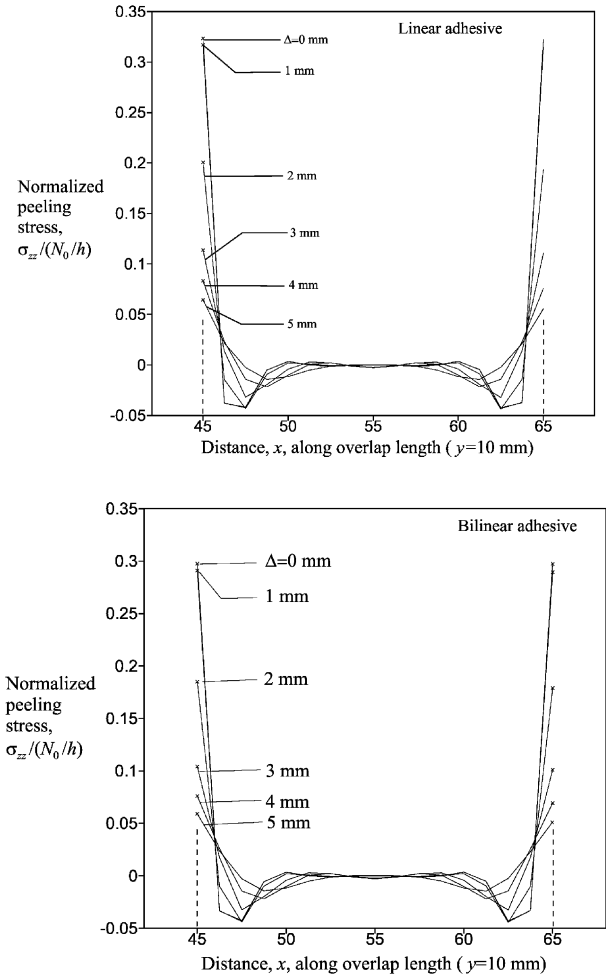

Fig. 9. Variation of the peeling stress, σ_{zz}, along the horizontal centerline for varying adherend taper lengths: linearly elastic and bilinear adhesive behavior.

and adhesive automatically limits the accuracy of the results to a degree less than the exact behavior of the bonded joint, the present solution method successfully captures, at least, the steep variation of the shearing and peeling stresses along the adhesive edges as shown in Fig. 7.

A comparison of the slope variation at the center of the overlap as the load is increased for the present solution method with that of the nonlinear FEA with ANSYS indicates close agreement, as shown in Fig. 8. The small difference can be attributed to the modeling differences and the fact that FEA includes transverse shearing deformations in the adherends, as well as in the adhesive, whereas the present approach is based on the Kirchhoff plate theory, which excludes the transverse shear deformations in the adherends.

The capability of the present approach is demonstrated by considering a bonded composite single-lap joint of angle-ply laminates (adherends) as shown in Fig. 4a. The adherend length and width and the overlap length, as well as the loading and boundary conditions, are identical to those of the validation case except for the presence of tapered adherend edges. The lower and upper laminate edges are tapered (beveled) toward the adhesive edges, as shown in Fig. 4a, where $\Delta^{(1)}$ and $\Delta^{(2)}$ indicate the taper lengths of the upper and lower adherends, respectively.

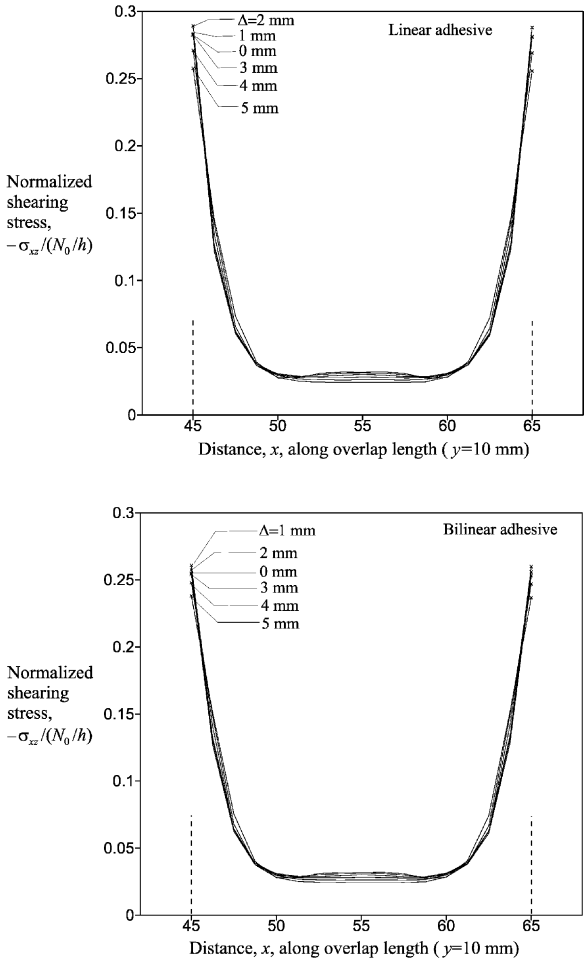

Fig. 10. Variation of the shearing stress, σ_{xz}, along the horizontal centerline for varying adherend taper lengths: linearly elastic and bilinear adhesive behavior.

Both adherends are symmetrically laminated and their angle-ply stacking sequence is given by $[\theta/-\theta]_{4s}$, where θ is referred to as the angle-ply laminate parameter. Each ply made of Graphite–Epoxy has properties of $E_L^{(p)} = 127.56$ GPa, $E_T^{(p)} = 11.31$ GPa, $v_{LT}^{(p)} = 0.3$, and $G_{LT}^{(p)} = 6.0$ GPa with equal nominal ply thicknesses of $t_k^{(p)} = 0.0762$ mm, with $p = 1,2$. Hence, the total thickness of the untapered laminate becomes $2h^{(p)} = h = 1.2192$ mm. The thickness of the adhesive is specified as $2h^{(1,2)} = 0.12$ mm. The linearly elastic behavior of the adhesive is defined by a shear modulus of $G_1^{(1,2)} = G_2^{(1,2)} = G^{(1,2)} = 0.4147$ GPa, and the bilinear adhesive material behavior is defined by the parameters $G_1^{(1,2)} = 0.4147$ GPa and $G_2^{(1,2)} = 300.$ MPa with a characteristic shear strain of $\gamma_c^{(1,2)} = 0.03$.

The effects of the tapered adherend geometry and the angle-ply laminate parameter, θ, on the geometrically nonlinear behavior of the bonded lap joint are investigated by (1) varying the taper lengths, $\Delta^{(1)}$ and $\Delta^{(2)}$, from 0 to 5 mm in five equal increments while specifying the value of $\theta = 45°$ (i.e, $[+45/-45]_{4s}$

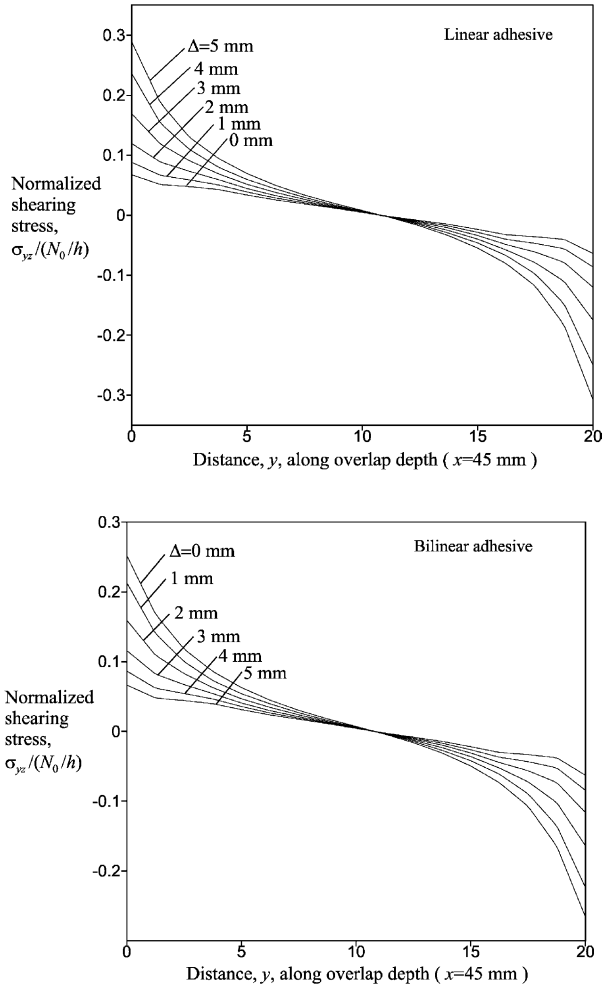

Fig. 11. Variation of the shearing stress, σ_{yz}, along the vertical centerline for varying adherend taper lengths: linearly elastic and bilinear adhesive behavior.

laminate), and (2) by varying the angle-ply laminate parameter, θ, as 0°, 5°, 10°, 15°, 30°, and 45° while assuming an untapered adherend edge, i.e., $\Delta^{(1)} = \Delta^{(2)} = 0$.

The effects of taper lengths on the transverse normal stress, σ_{zz}, and the transverse shear stress, σ_{xz}, both evaluated along the horizontal centerline $y = 10$ mm, are depicted in Figs. 9 and 10, respectively, for both linearly elastic and bilinear adhesive material behaviors. As shown in these figures, the peeling stress, σ_{zz}, reduces with increasing taper length, and the shearing stress, σ_{xz}, reduces slightly along the horizontal centerline of the adhesive. The transverse shear stress, σ_{yz}, evaluated along the vertical centerline ($x = 45$ mm line) is depicted in Fig. 11, also for both linearly elastic and bilinear adhesive material behaviors. The shear stress component near the corners of the adhesive edges decreases significantly with increasing taper length. Although not shown here, the transverse shearing stress, σ_{xz}, also reduces significantly at the corners of the adhesive edges as a result of increasing taper length. As observed in Figs. 9–11, the bilinear adhesive material behavior yields stress variations identical to those of the linear adhesive behavior, but with relatively lower transverse normal and shear stress variations than those of the linearly elastic adhesive material.

Variations of the peeling stress, σ_{zz}, and transverse shear stresses, σ_{xz} and σ_{yz}, at the final load step, $N_0/N_0^{\max} = 1.0$, in the adhesive with linearly elastic adhesive material in the absence of tapered adherend

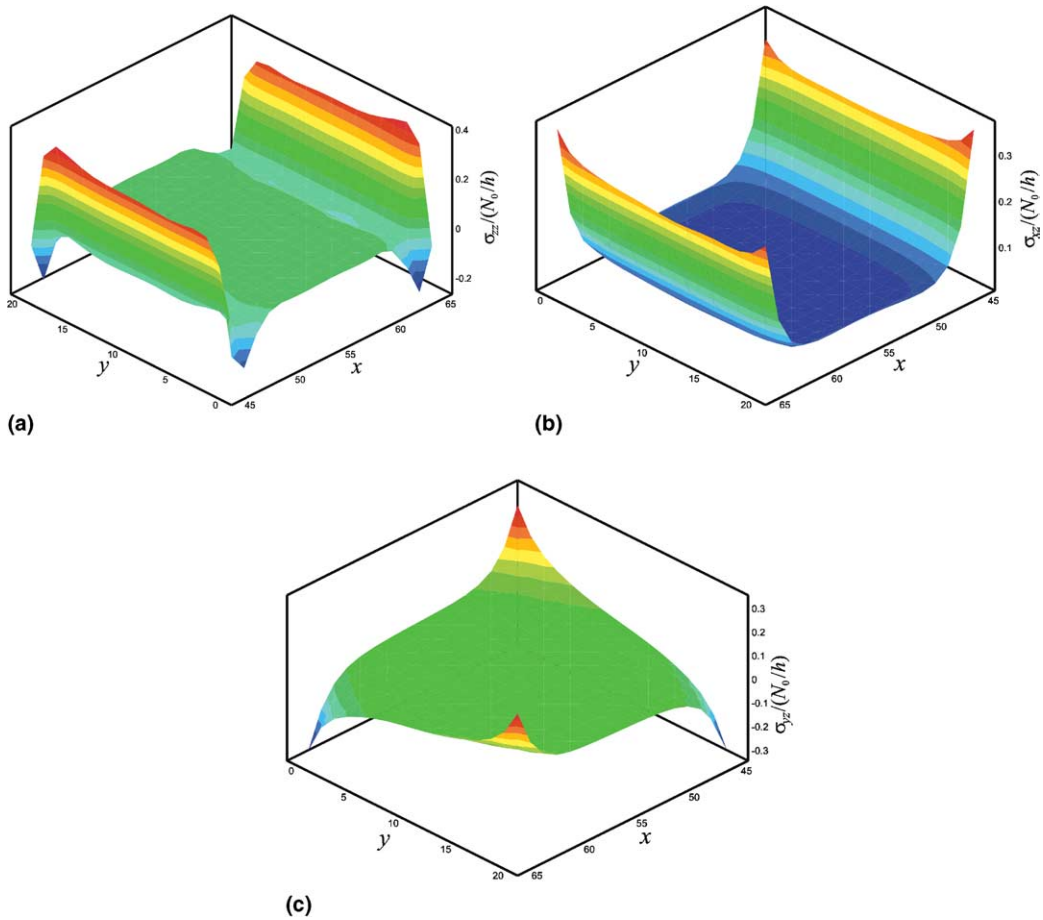

Fig. 12. Variation of the stress components in the adhesive: (a) peeling stress, σ_{zz}, (b) shearing stress, σ_{xz} along the horizontal vertical centerline, and (c) shearing stress, σ_{yz} for untapered adherends of $[\pm 45]_{4s}$ angle-ply laminates with linear adhesive behavior.

edges are illustrated in Fig. 12. As expected, both the transverse shear and peeling stresses increase rapidly near the edges of the adhesive. As observed in Fig. 12, all of the adhesive stress variations are asymmetric with respect to the horizontal and vertical centerlines. Although the adherents are symmetric angle-ply laminates with no material coupling between stretching and bending that may cause twisting in the adherends and result in asymmetric stress distribution in the adhesive, the coupling between the bending and twisting deformations disturbs the symmetry in the adhesive stresses.

In order to understand this behavior, the adhesive stresses are evaluated along the left edge of the adhesive (i.e., $x = 45$) for varying angle-ply laminate parameter, θ, as shown in Fig. 13. These results are obtained for untapered adherends and linearly elastic adhesive behavior. As shown in Fig. 13a, the peeling stress, σ_{zz}, is symmetric along the adhesive edge for $\theta = 0$. As θ is gradually increased from 0° to 15°, the peeling stress near the upper corner of the left adhesive edge (i.e., $x = 45$ and $y = 20$) becomes higher than that near the lower corner (i.e., $x = 45$ and $y = 0$). As θ is further increased, the difference in the peeling stress near the corners of the adhesive edge becomes more pronounced, as shown in Fig. 13a. A similar behavior is also observed in the transverse shearing stress, σ_{xz}, where the magnitude of stress at one corner

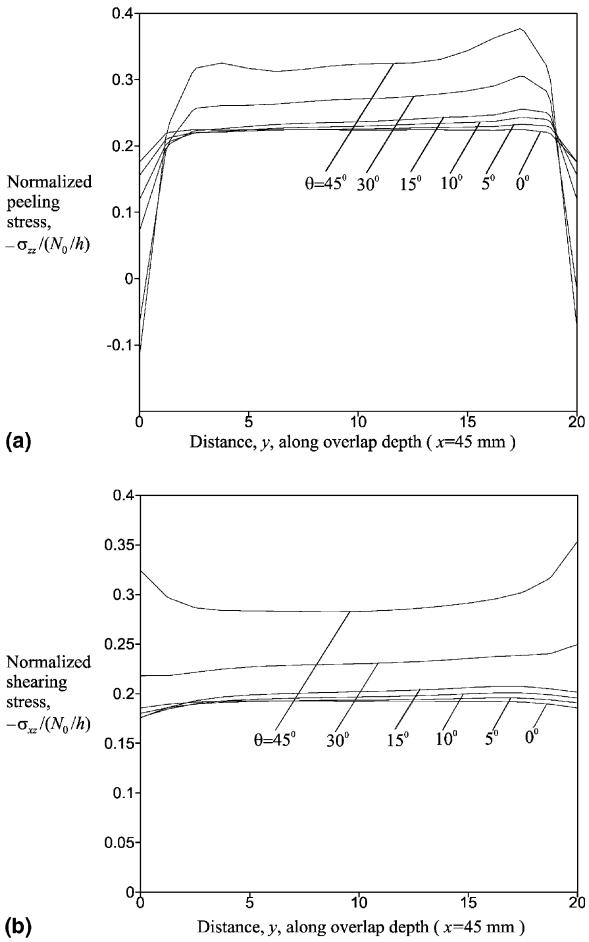

Fig. 13. Variation of stress components in the adhesive with bi-linear material behavior: (a) peeling stress, σ_{zz}, and (b) shearing stress, σ_{xz}, along the left edge of the adhesive for varying values of angle-ply parameter, θ.

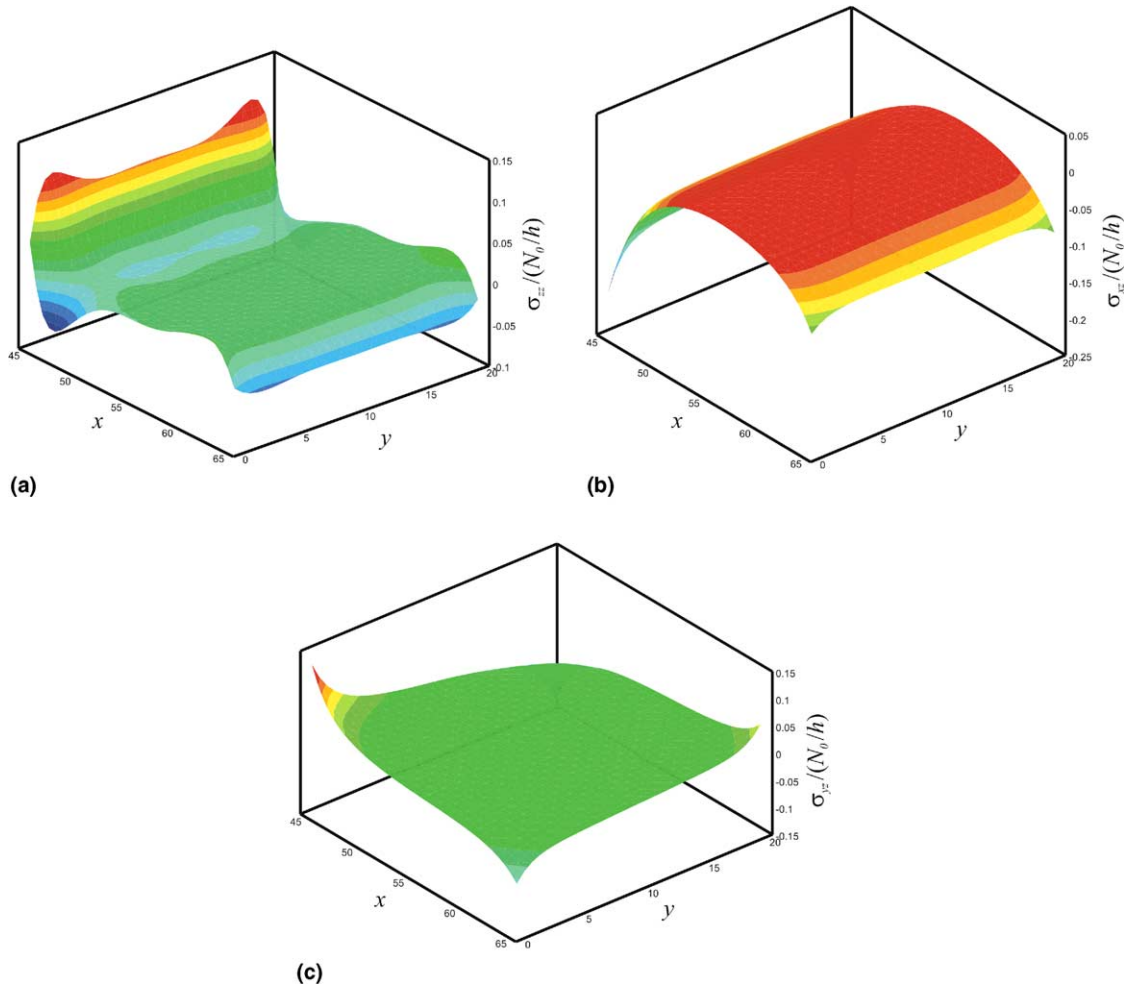

Fig. 14. Variation of the stress components in the first adhesive: (a) peeling stress, σ_{zz}; (b) shearing stress, σ_{xz}; and (c) shearing stress, σ_{yz} with linear adhesive behavior.

Fig. 15. Scaled deformation of the bonded double-lap joint at the last load step.

is different than that at the other corner, as shown in Fig. 13b. Both the peeling and shearing stresses increase with increasing θ. This is primarily due to the reduction of adherend in-plane and bending stiffnesses in the longitudinal direction. The lower the in-plane and bending stiffnesses of the adherends the higher the edge effects.

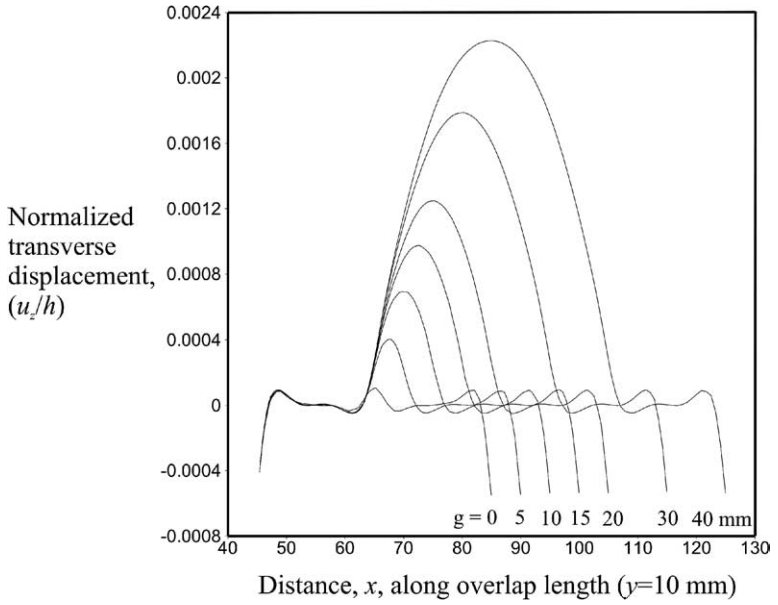

Fig. 16. Out-of-plane displacement of the lower adherend as a function of gap length.

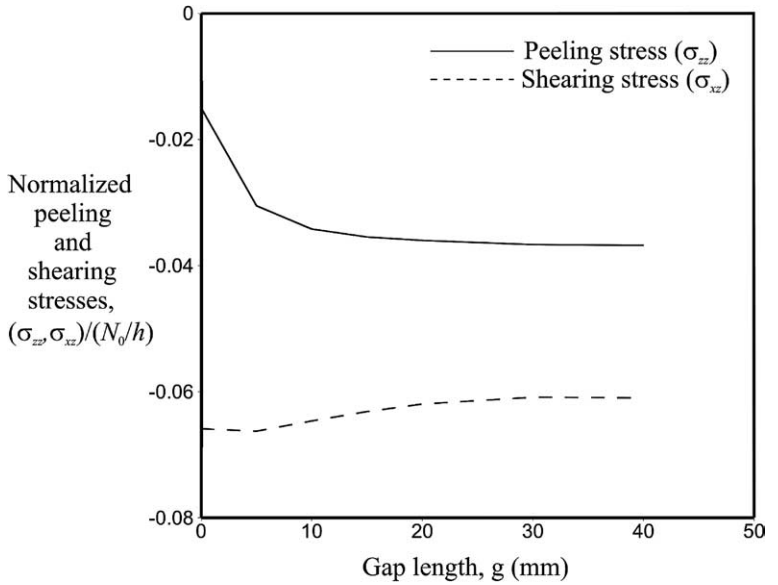

Fig. 17. Variation of the peeling, σ_{zz}, and shearing, σ_{xz}, stress components at the mid-point of the inner adhesive edge as a function of gap length with linear adhesive behavior.

The capability of the present approach is further demonstrated by considering a bonded composite double-lap joint of angle-ply laminates (adherends) without tapered edges. As shown in Fig. 4b, the width and length of the adherends are specified as $W^{(p)} = W = 20$ mm, with $p = 1, 2, 3, 4$ and $L^{(1)} = L^{(2)} = 65$ mm and $L^{(3)} = L^{(4)} = 50$ mm, respectively. The overlap (adhesive) length between the adherends is specified as $L^{(1,3)} = L^{(1,4)} = L^{(2,3)} = L^{(2,4)} = 20$ mm. The thicknesses of the adherends and the adhesives are specified as $2h^{(p)} = h = 1.2192$ mm and $2h^{(1,3)} = 2h^{(1,4)} = 2h^{(2,3)} = 2h^{(2,4)} = 0.12$ mm, respectively.

Adherends are symmetrically laminated and their angle-ply stacking sequence is given by $[30/-30]_{4s}$. Ply and adhesive properties as well as their thicknesses are same as those defined for the single-lap joint. The double-lap joint is simply supported along the loaded ends and subjected to uniform tension of $N_0 = 100$ N/mm in 10 equal load increments.

The variations of the peeling stress, σ_{zz}, and transverse shear stresses, σ_{xz} and σ_{yz}, in the adhesive with linearly elastic adhesive material behavior obtained at the final load step of $N_0/N_0^{\max} = 1.0$ are illustrated in

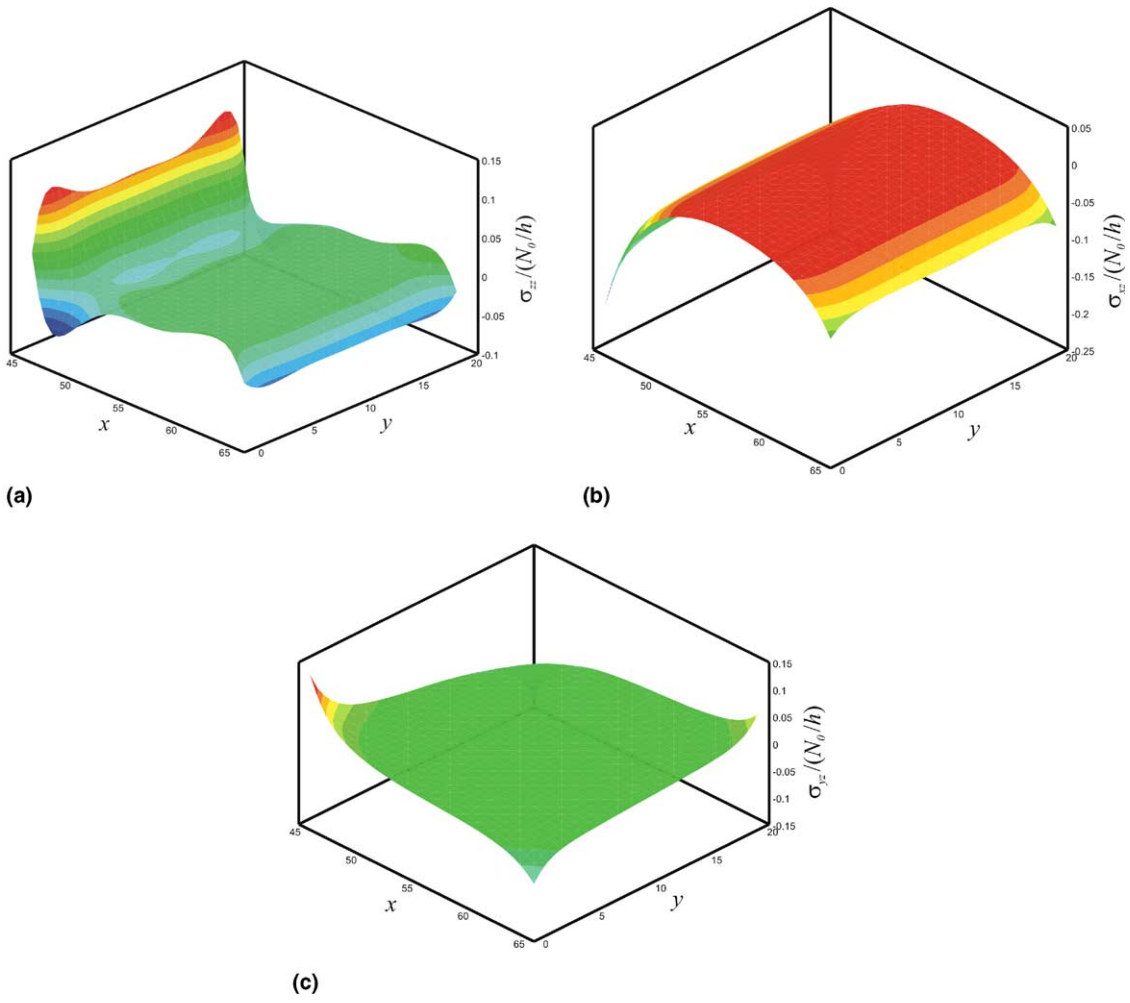

Fig. 18. Variation of the stress components in the first adhesive: (a) peeling stress σ_{zz}; (b) shearing stress σ_{xz}; and (c) shearing stress σ_{yz} with bilinear adhesive behavior.

Fig. 14. The peeling (σ_{zz}) and shearing (σ_{xz}) stress distributions depicted in Fig. 14a and b reveal that bending deformation occurs in the upper and lower adherends (adherends 3 and 4) even though the adherends are both symmetrically laminated and placed with respect to each other. This observation is also verified by the out-of-plane deformed configuration of the adherends in Fig. 15, in which the upper and lower adherends (adherends 3 and 4) have curvatures while the centerline adherends (adherends 1 and 2) remain straight after deformation.

The bending deformations in the upper and lower adherends cause tensile and compressive peeling stress distributions along the outer and inner adhesive edges, respectively as captured in Fig. 14a. Furthermore, the tensile peeling stress distributions along the outer edges of the adhesive regions are relatively higher in magnitude than the compressive peeling stresses along the inner edges. This expected behavior is mainly due to the presence of the gap between the center adherends that result in stress concentrations along the inner adhesive edges. As shown in Fig. 16, the out-of-plane displacement variation at the center of lower and upper adherents considerably increase with increasing gap length as a result of the bending action taking place when the tensile in-plane loads are eccentrically transferred to these upper and lower adherends from the center adherends. Also, Fig. 17 demonstrates the effect of the gap length on the peeling (σ_{zz}) and shearing (σ_{xz}) stresses evaluated at the mid point on the inner edges. While the peeling stresses increase considerably with increasing gap length, the shearing stress evaluated at these points slightly decrease as the gap length increases. The nearly steady variation of the shearing stress is expected because the in-plane load transfer between the center adherends and the lower and upper adherends always causes shear stress concentrations to develop along the vertical edges of the adhesive layers regardless of the presence of the gap.

In the case of bilinear adhesive behavior, the variations of the peeling stress, σ_{zz}, and transverse shear stresses, σ_{xz} and σ_{yz}, at the final load step are illustrated in Fig. 18. The peeling and shearing stress distributions given in these figures exhibit behavior similar to those linearly elastic adhesive material behavior, except for the magnitudes of the peeling and shearing stresses being slightly lower in the regions where the adhesive stresses exceed their corresponding critical strains.

5. Conclusions

A semi-analytical solution procedure was presented for the geometrically nonlinear three-dimensional analysis of a single- and double-lap joints made of composite tapered adherends bonded by a linearly elastic or bilinear adhesive. The nonlinear equations of equilibrium were derived based on the principle of virtual displacements in conjunction with the von Karman nonlinear plate theory for the adherends and the shear-lag theory for the adhesive. The bilinear adhesive material behavior was incorporated by computing the material parameters from an effective shear stress-shear strain relationship. The displacement fields were assumed in the form of a double series containing fifth-order B-spline functions (displacement modes) in each direction. The resulting nonlinear equations of equilibrium were then solved numerically by employing the Newton–Raphson incremental iterative procedure along with Broyden's automatic Jacobian matrix update.

A comparison against a two-dimensional nonlinear FEA solution established the capability of the present approach to accurately capture the steep variations of both peeling and shearing stresses in the vicinity of the adhesive edges, as well as at the corners. Furthermore, the variation of overlap rotations indicates that the stress-induced effects due to geometric nonlinearity were captured by preserving the nonlinear terms in the strain displacement relations.

In the case of a bonded single-lap joint of angle-ply laminates, the tapered edges led to a considerable reduction of the peeling stresses and a slight reduction of the shearing stress component in the longitudinal direction (σ_{xz}). However, the increase in taper length reduced all the adhesive stress components at the

corners of the adhesive region. Furthermore, the increase in the angle-ply laminate parameter not only increased the stress concentration near the adhesive edges but also changed the symmetric distribution of peeling and longitudinal (transverse) shearing stresses to asymmetric due to the presence of material coupling between bending and twisting deformations of the angle-ply laminates.

In the case of a bonded double-lap joint, the present analysis also captures the influence of the gap between the center adherends on the bending behavior of the patches (lower and upper adherends) and especially the stress distribution in the adhesive layers between these adherends. As the upper and lower adherends bend due to the presence of the gap, they tend to pull the center adherends near the outer overlap edges and push along the inner edges, thus creating tensile and compressive peeling stresses along these edges, respectively. Also, stress concentrations of both peeling and shearing stresses appear along the inner adhesive edges. The peeling stresses along the inner edges increase with increasing gap size. However, no noticeable difference is obtained in the shearing stress calculations along the inner edges as a result of increasing gap length.

Appendix A

The B-spline functions, $T_m(\alpha;\mathbf{t}_\alpha^{(p)},K)$, with $\alpha = x, y$ and $(p = 1,\ldots,P)$, employed in Eq. (8) are defined recursively in the form (Hoschek and Lasser, 1993)

$$T_m(\alpha;\mathbf{t}_\alpha^{(p)},K) = \frac{(\alpha - t^{(p)}_{\alpha(m)})}{\left(t^{(p)}_{\alpha(m+K-1)} - t^{(p)}_{\alpha(m)}\right)} T_m(\alpha;\mathbf{t}_\alpha^{(p)},K-1) + \frac{\left(t^{(p)}_{\alpha(m+K)} - \alpha\right)}{\left(t^{(p)}_{\alpha(m+K)} - t^{(p)}_{\alpha(m+1)}\right)} T_{m+1}(\alpha;\mathbf{t}_\alpha^{(p)},K-1) \tag{72}$$

with $m = 1,2,\ldots,M_\alpha^{(p)}$ and $k > 1$. The variable $t^{(p)}_{\alpha(m)}$ represents the components of the knot vector, $\mathbf{t}_\alpha^{(p)}$, for the $(K-1)$th-degree B-spline functions. The knot vector, $\mathbf{t}_\alpha^{(p)}$, is defined in terms of the Cartesian coordinate $(\alpha = x, y)$ of the selected points as

$$\begin{aligned}\mathbf{t}_\alpha^{(p)} &= \left\{t^{(p)}_{\alpha(0)}, t^{(p)}_{\alpha(1)},\ldots,t^{(p)}_{\alpha(N_\alpha^{(p)})}, t^{(p)}_{\alpha(N_\alpha^{(p)}+1)}, t^{(p)}_{\alpha(N_\alpha^{(p)}+2)},\ldots,t^{(p)}_{\alpha(N_\alpha^{(p)}+2K)}\right\} \\ &= \left\{\alpha_0^{(p)},\alpha_0^{(p)},\ldots,\alpha_0^{(p)},\alpha_1^{(p)},\alpha_2^{(p)},\ldots,\alpha^{(p)}_{N_\alpha^{(p)}},\alpha^{(p)}_{N_\alpha^{(p)}+1},\alpha^{(p)}_{N_\alpha^{(p)}+1},\ldots,\alpha^{(p)}_{N_\alpha^{(p)}+1}\right\}\end{aligned} \tag{73}$$

where $N_\alpha^{(p)} + 1 (\alpha = x, y; p = 1,\ldots,P)$ denotes the number of distinct knot points selected along the α direction in the lower and upper adherends. Based on the definition of the knot vector, $\mathbf{t}_\alpha^{(p)}$, the end points (i.e., $\alpha_0^{(p)}$ and $\alpha^{(p)}_{N_\alpha^{(p)}+1}$) are repeated K times. In Eqs. (72) and (73), the relationship between the number of knot points and the extent of the B-spline functions, $M_\alpha^{(p)}$, is given as

$$M_\alpha^{(p)} = N_\alpha^{(p)} - K + 3 \tag{74}$$

In this study, the knot point numbers, $N_\alpha^{(p)}$ and $M_\alpha^{(p)}$ in the x- and y-directions, respectively are varied in the B-spline functions with $K = 5$.

Appendix B

The nonlinear equilibrium equation, Eq. (70), can be rearranged in the form

$$\boldsymbol{\psi}(\mathbf{q}) = \mathbf{K}(\mathbf{q})\mathbf{q} - \mathbf{f} = \mathbf{0} \tag{75}$$

where the vectors $\mathbf{q}$ and $\mathbf{f}$ and the matrix $\mathbf{K}(\mathbf{q})$ are defined as

$$\mathbf{q}^{\mathrm{T}} = \left\{ \mathbf{q}^{(1)^{\mathrm{T}}}, \mathbf{q}^{(2)^{\mathrm{T}}}, \ldots, \mathbf{q}^{(r)^{\mathrm{T}}}, \lambda^{(1)^{\mathrm{T}}}, \ldots, \lambda^{(2)^{\mathrm{T}}}, \lambda^{(r)^{\mathrm{T}}} \right\} \tag{76a}$$

$$\mathbf{f}^{\mathrm{T}} = \left\{ \mathbf{p}^{(1)^{\mathrm{T}}}, \mathbf{p}^{(2)^{\mathrm{T}}}, \ldots, \mathbf{p}^{(r)^{\mathrm{T}}}, \mathbf{f}_c^{(1)^{\mathrm{T}}}, \mathbf{f}_c^{(2)^{\mathrm{T}}}, \ldots, \mathbf{f}_c^{(r)^{\mathrm{T}}} \right\} \tag{76b}$$

$$\mathbf{K}(\mathbf{q}) = \begin{bmatrix} \mathbf{K}_{11} & \mathbf{K}_{12} & \ldots & \mathbf{K}_{1P} & \mathbf{C}^{(1)^{\mathrm{T}}} & \mathbf{0} & \cdots & \mathbf{0} \\ \mathbf{K}_{12}^{\mathrm{T}} & \mathbf{K}_{22} & \ldots & \mathbf{K}_{2P} & \mathbf{0} & \mathbf{C}^{(2)^{\mathrm{T}}} & \cdots & \mathbf{0} \\ \vdots & \vdots & \vdots & \vdots & \vdots & \vdots & \vdots & \vdots \\ \mathbf{K}_{1P}^{\mathrm{T}} & \mathbf{K}_{2P}^{\mathrm{T}} & \cdots & \mathbf{K}_{PP} & \mathbf{0} & \mathbf{0} & \mathbf{0} & \mathbf{C}^{(P)^{\mathrm{T}}} \\ \mathbf{C}^{(1)} & \mathbf{0} & \cdots & \mathbf{0} & \mathbf{0} & \mathbf{0} & \cdots & \mathbf{0} \\ \mathbf{0} & \mathbf{C}^{(2)} & \cdots & \mathbf{0} & \mathbf{0} & \mathbf{0} & \cdots & \mathbf{0} \\ \vdots & \vdots & \vdots & \vdots & \vdots & \vdots & \vdots & \vdots \\ \mathbf{0} & \mathbf{0} & \mathbf{0} & \mathbf{C}^{(P)} & \mathbf{0} & \mathbf{0} & \mathbf{0} & \mathbf{0} \end{bmatrix} \tag{76c}$$

The vector $\boldsymbol{\psi}(\mathbf{q})$ represents the unbalanced load vector. Under equilibrium conditions, the solution vector $\mathbf{q}$ exactly satisfies Eq. (75) and no unbalanced forces exist. However, it is practically impossible to obtain a direct solution of the nonlinear equilibrium equations. Instead, the solution is obtained by resorting to an iterative procedure such as the Newton–Raphson (N–R) method. In order to proceed with the N–R method, Eq. (75) is rewritten in iterative form as

$$\boldsymbol{\psi}(\mathbf{q}_m^{k+1}) = \mathbf{K}(\mathbf{q}_m^{k+1})\mathbf{q}_m^{k+1} - \mathbf{f}_m = \mathbf{0} \tag{77}$$

where $\mathbf{q}_m^{k+1}$ denotes the trial solution vector at load step m after k number of iterations, and it is expressed as a correction to the trial solution vector, $\mathbf{q}_m^k$, at the kth iteration at load step m, i.e.,

$$\mathbf{q}_m^{k+1} = \mathbf{q}_m^k + \Delta\mathbf{q} \tag{78}$$

in which $\Delta\mathbf{q}$ represents the correction term (incremental solution vector). The solution vector $\mathbf{q}_m^k$ is known from the kth iteration at load step m and the correction term, $\Delta\mathbf{q}$ is to be determined.

The Taylor series expansion of $\boldsymbol{\psi}(\mathbf{q}_m^{k+1})$ about the known trial solution $\mathbf{q}_m^k$ as

$$\boldsymbol{\psi}(\mathbf{q}_m^{k+1}) = \boldsymbol{\psi}(\mathbf{q}_m^k) + \frac{\partial \boldsymbol{\psi}}{\partial \mathbf{q}}(\mathbf{q}_m^k)\Delta\mathbf{q} + \mathrm{HOT} = 0 \tag{79}$$

in which the unbalanced load vector $\boldsymbol{\psi}(\mathbf{q}_m^k)$ is non-zero from the kth trial solution vector, $\mathbf{q}_m^k$. Retaining the linear terms in the expansion while disregarding the higher order terms (HOT), the Newton–Raphson (N–R) method yields

$$\mathbf{J}(\mathbf{q}_m^k)\Delta\mathbf{q} = -\boldsymbol{\psi}(\mathbf{q}_m^k) \tag{80}$$

where the Jacobian matrix, $\mathbf{J}(\mathbf{q}_m^k)$, is defined as

$$\mathbf{J}(\mathbf{q}_m^k) = \frac{\partial \boldsymbol{\psi}}{\partial \mathbf{q}}(\mathbf{q}_m^k) = \frac{\partial \mathbf{K}}{\partial \mathbf{q}}(\mathbf{q}_m^k)\mathbf{q}_m^k + \mathbf{K}(\mathbf{q}_m^k) \tag{81}$$

and

$$\Delta\mathbf{q} = \mathbf{q}_m^{k+1} - \mathbf{q}_m^k \tag{82}$$

Because of the linearization of Eq. (78), the incremental solution vector (the correction term), $\Delta\mathbf{q}$ obtained from Eq. (79) is not expected to yield the actual solution. However, it provides a good estimate of $\mathbf{q}_m^{k+1}$ in the form

$$\mathbf{q}_m^{k+1} = \mathbf{q}_m^k - \mathbf{J}^{-1}(\mathbf{q}_m^k)\boldsymbol{\psi}(\mathbf{q}_m^k) \tag{83}$$

As part of the iterative solution procedure, this recursive relationship requires the updated Jacobian matrix, i.e., $\mathbf{J}(\mathbf{q}_m^{k+1})$, which is obtained based on Broyden's algorithm (Geradin et al., 1981)

$$\mathbf{J}(\mathbf{q}_m^{k+1}) = \mathbf{J}(\mathbf{q}_m^k) + \frac{\left[\Delta\boldsymbol{\psi} - \mathbf{J}(\mathbf{q}_m^k)\Delta\mathbf{q}\right]\Delta\mathbf{q}^{\mathrm{T}}}{\Delta\mathbf{q}^{\mathrm{T}}\Delta\mathbf{q}} \tag{84}$$

where

$$\Delta\boldsymbol{\psi} = \boldsymbol{\psi}(\mathbf{q}_m^{k+1}) - \boldsymbol{\psi}(\mathbf{q}_m^k) \tag{85}$$

At the beginning of current (mth) load step, the converged solution vector, $\mathbf{q}_{m-1}^k$, and the Jacobian matrix, $\mathbf{J}(\mathbf{q}_{m-1}^k)$, computed from the previous load step are employed as the initial estimates for the solution vector and the Jacobian matrix in the current load step, i.e.,

$$\mathbf{q}_m^0 = \mathbf{q}_{m-1}^k = \mathbf{q}_{m-1} \text{ and } \mathbf{J}(\mathbf{q}_m^0) = \mathbf{J}(\mathbf{q}_{m-1}^k) = \mathbf{J}(\mathbf{q}_{m-1}) \tag{86a, b}$$

where the superscripts on the right hand sides of Eqs. (86) are removed to represent the converged solutions from the preceding load step.

Note that for the case of $k = m = 0$ (i.e., $\mathbf{q}_0^0 = \mathbf{0}$), the Jacobian matrix $\mathbf{J}(\mathbf{q}_0^0 = \mathbf{0})$ represents the linear stiffness matrix at the unloaded state of the bonded lap joint, i.e.,

$$\mathbf{J}(\mathbf{q}_0^0 = \mathbf{0}) = \mathbf{K}(\mathbf{q}^{(1)} = 0, \ldots, \mathbf{q}^{(P)} = 0) = \mathbf{K}_L \tag{87}$$

Therefore, the initial solution vector and the Jacobian matrix in the first load step are estimated by

$$\mathbf{q}_1^0 = \mathbf{0} \text{ and } \mathbf{J}(\mathbf{q}_1^0) = \mathbf{K}_L \tag{88}$$

References

Apalak, M.K., Gunes, R., 2001. On nonlinear thermal stresses in an adhesively bonded single lap joints. Computers and Structures 80, 85–98.

Dattaguru, B., Everett Jr., R.A., Whitcomb, J.D., Johnson, W.S., 1984. Geometrically nonlinear analysis of adhesively bonded joints. Journal of Engineering Materials and Technology 106, 59–65.

Ding, S., Kumosa, M., 1994. Singular stress behavior at an adhesive interface corner. Engineering Fracture Mechanics 47, 503–519.

Edlund, U., Klarbring, A., 1992. A geometrically nonlinear model of the adhesive joint problem and its numerical treatment. Computer Methods in Applied Mechanical Engineering 96, 329–350.

Fung, Y.C., Tong, P., 2001. Classical and Computational Solid Mechanics. World Scientific Publishing Co. Pte. Ltd., Singapore.

Geradin, M., Idelsohn, S., Hogge, M., 1981. Computational strategies for the solution of large nonlinear problems via quasi-Newton methods. Computers and Structures 13, 73–81.

Goland, M., Reissner, E., 1944. The stresses in cemented joints. Journal of Applied Mechanics 66, A17–A27.

Hoschek, J., Lasser, D., 1993. Fundamentals of Computer Aided Geometric Design. A K Peters, Ltd., Wellesley, MA.

Narasimhan, S., Pandey, P.C., 2003. Three-dimensional material and geometrical nonlinear analysis of adhesively bonded single-lap joints. Defense Science Journal 53, 175–188.

Osnes, H., Andersen, A., 2003. Computational analysis of geometric nonlinear effects in adhesively bonded single lap composite joints. Composites Part B 34, 417–427.

Pandey, P.C., Narasimhan, S., 2001. Three-dimensional nonlinear analysis of adhesively bonded lap joints considering viscoplasticity in adhesives. Computers and Structures 79, 769–783.

Pandey, P.C., Shankaragouda, H., Singh, A.K., 1999. Nonlinear analysis of adhesively bonded lap joints considering viscoplasticity in adhesives. Computers and Structures 70, 387–413.

Penado, F.E., 1998. A simplified method for the geometrically nonlinear analysis of the single-lap joint. Journal of Thermoplastic Composite Materials 11, 272–287.

Reddy, J.N., Roy, S., 1988. Non-linear analysis of adhesively bonded joints. International Journal of Non-Linear Mechanics 23, 97–112.

Tsai, M.Y., Morton, J., 1994. An evaluation of analytical and numerical solutions to the single-lap joint. International Journal of Solids and Structures 31, 2537–2563.